CONCENTRATION MEASUREMENTS OF AN INJECTED GAS IN A SUPERSONIC STREAM

LANGLEY RESEARCH CENTER
HAMPTON, VA

APRIL 67

NASA TECHNICAL NOTE NASA TN D-3860

NASA TN D-3860

CONCENTRATION MEASUREMENTS OF AN INJECTED GAS IN A SUPERSONIC STREAM

by Marvin G. Torrence

Langley Research Center
Langley Station, Hampton, Va.

NATIONAL AERONAUTICS AND SPACE ADMINISTRATION • WASHINGTON, D. C. • APRIL 1967

NASA TN D-3860

CONCENTRATION MEASUREMENTS OF AN INJECTED GAS IN A SUPERSONIC STREAM

By Marvin G. Torrence

Langley Research Center
Langley Station, Hampton, Va.

NATIONAL AERONAUTICS AND SPACE ADMINISTRATION

For sale by the Clearinghouse for Federal Scientific and Technical Information
Springfield, Virginia 22151 – CFSTI price $3.00

CONCENTRATION MEASUREMENTS OF AN INJECTED GAS IN A SUPERSONIC STREAM

By Marvin G. Torrence
Langley Research Center

SUMMARY

An experimental investigation has been made by using a tracer-gas technique for injected-gas concentration measurements and to obtain preliminary mixing data. The injected gas was a 1-percent mixture of ethane in air. Mass-fraction concentration (air in air) distributions have been determined and static- and total-pressure measurements have been made downstream of a sonic jet, which issued normal to a supersonic stream from the surface of a flat plate. Surveys were made at axial stations of 7, 15, and 30 jet diameters and at jet- to free-stream total-pressure ratios of 0.34 and 0.60. This experiment was conducted at a free-stream Mach number of 4.03 and a Reynolds number per meter of 7.87×10^7. Stagnation conditions of pressure and temperature were 17 atmospheres and 300°K, respectively.

INTRODUCTION

The study of secondary injection into a supersonic stream has become the subject of considerable research effort. Some of the analytical and experimental work in this area is reported in references 1 to 6. In addition to side-force effects for thrust-vector control, secondary injection is of importance in combustion and heat-transfer application. Mixing of an injected gaseous fuel in combustible proportions, although desirable in combustion chambers, is usually undesirable when the fuel is vented from a flight vehicle. In the case of the multistage chemical rocket using a cryogenic propellant such as hydrogen, large quantities of waste gaseous fuel must be vented overboard. After the waste gas is dumped overboard, it may be exposed to regions of high temperature such as surface boundary layer and the nozzle base area of the operating first-stage engine. The current approach to the alleviation of this problem is the piping of the vented gas to the exhaust region of the first-stage engine. This solution imposes a weight penalty and problems associated with piping disconnects necessary for stage separation. An alternate solution is the venting of the gas in such a manner that the mixture is diluted below the lower limit of flammability in a reasonably short distance from the point of injection. Theoretical prediction of the mixing process and concentration distribution is extremely difficult and

creates a demand for experimental data to determine the governing parameters of the process.

An experimental investigation has been made by using a tracer-gas technique to obtain preliminary mixing data. The injected gas was a mixture of approximately 1 percent by volume of ethane in air. Mass-fraction concentration distributions have been determined downstream of a sonic jet issuing normal to a supersonic stream from the surface of a flat plate. This region was also surveyed to determine static- and total-pressure distributions. Surveys were made at downstream axial stations of 7, 15, and 30 jet diameters and at jet- to free-stream total-pressure ratios of 0.34 and 0.60. The tests were conducted at a free-stream Mach number of 4.03 and a Reynolds number per meter of 7.87×10^7. Tunnel stagnation conditions of pressure and temperature were 17 atmospheres and 300° K, respectively.

SYMBOLS

γ	ratio of specific heats
D	jet diameter, meters
G	mass flow per unit cross-sectional area, $\frac{\text{kilograms}}{\text{meter}^2\text{-second}}$
h	penetration height, meters
K	mass fraction of injected gas, $\frac{m_{j,x}}{m_{mix}}$
B	mole fraction of injected gas
M	Mach number
$\mathcal{M}$	molecular weight
m	mass, kilograms
p	absolute pressure, $\frac{\text{newtons}}{\text{square meter}}$
ρ	mass density, $\frac{\text{kilograms}}{\text{meter}^3}$
T	temperature, °Kelvin

V	velocity, $\frac{\text{meters}}{\text{second}}$
x	longitudinal coordinate
y	lateral coordinate
z	vertical coordinate
$\xi = K\left(\frac{G_x}{G_j}\right)$	
θ	injection angle measured from vertical

Subscripts:

∞	free-stream conditions
t	stagnation conditions
max	maximum value
w	plate surface conditions
x	survey point
j	injected gas
mix	mixture of injected and free-stream gases

MODEL AND TEST FACILITY DESCRIPTION

The model, shown in figure 1, consisted of a rectangular flat plate containing a flush-mounted sonic orifice located normal to the plate surface. Details of the jet nozzle orifice are shown in section B-B of figure 1. The underside of the plate consists of a 2° wedge at the leading edge followed by a 10° wedge. The forward wedge tapers to a cylindrical leading edge of approximately 0.0127-centimeter thickness. Boundary-layer pressure surveys at the jet station with no injection indicate a turbulent boundary layer with a thickness of approximately 3 jet diameters.

The facility used in these tests was a continuous-flow supersonic tunnel with the model spanning the 23-cm by 23-cm test section. The tunnel exhausted to the atmosphere and utilized two-dimensional fixed-geometry nozzle blocks and a second minimum followed by a subsonic diffuser. Schlieren observations and wall pressure measurements indicated the formation of weak shock waves in the tunnel test section upstream of the model jet station. The Mach number above the boundary layer on the flat plate at the jet station was 4.03. All test runs were made by using dry air at tunnel stagnation conditions of 17 atmospheres and 300° K. The unit Reynolds number was 7.87×10^7 per meter.

Secondary Flow

The secondary flow routing is shown schematically in figure 2. The main jet flow, piped from the settling chamber ahead of the tunnel throat, was metered and regulated to the selected jet test pressure. Ethane tracer gas was then metered into the air line at a flow rate corresponding to a 1-percent volumetric mixture. Immediately downstream of the point of tracer introduction, a chamber was installed to insure complete mixing of the jet air and tracer gas before injection into the tunnel flow. The mixing chamber consisted of a series of four disk baffles with staggered hole passages that provided a minimum flow-path length in the chamber of approximately 20 inlet pipe diameters. Passage area was increased in each successive baffle to insure noncritical flow in the chamber. An iron-constantan thermocouple was installed in the exit end of the mixing chamber to measure jet total temperature. At a distance of approximately 62 pipe diameters below the mixing chamber, a total-pressure tube was installed in the jet flow line to measure jet stagnation pressure and to remove samples for chromatograph full-scale readings.

Instrumentation

Gas analyzer.- A process gas chromatograph was used to obtain the concentration data presented in this report. The fundamentals of gas chromatography can be found in reference 7. The chromatograph measures the volumetric concentration of each constituent of the sample. The components are separated when passed through a column consisting of a length of stainless-steel tubing packed with activated alumina. Since each component progresses through the column at a predictable rate, the travel time (or elution time) identifies each component qualitatively. Thermal conductivity detectors measure the quantity of each of the separated gases relative to the carrier gas and concentrations are printed out on a strip chart recorder. Readout controls were adjusted to eliminate the recording of all sample components except ethane. The chromatograph was calibrated before each test run and repeatability of the instrument checked to a variation of less than 1 percent of full scale.

Pressure measurements.- Survey static pressures were measured by a 5-psia (3.45×10^4 N/m^2) pressure transducer. To reduce response time lag, the transducer was placed in proximity of the tunnel and mounted to eliminate noise effects. An identical transducer, under a known pressure, was monitored during each test run, and indicated no error due to noise level in the test cell. Both transducers were calibrated before and after each test run. Pitot pressures were measured by ±25 psid ($\pm 1.724 \times 10^5$ N/m^2) and 0 to 50 psia (3.45×10^5 N/m^2) transducers. Both static and pitot pressures were recorded on automatic balance potentiometer recorders. Tunnel and jet stagnation conditions were measured with total-pressure probes and standard iron-constantan thermocouples.

The model wall static orifice coordinates are given in table I, the coordinate system origin being located at the jet center. Orifices were located along radial lines emanating from the jet center and pressures were measured by mercury manometers. Tunnel-sidewall static pressures were measured and a wall orifice at the axial survey position was used as a check on the probe static-pressure reading in the fully retracted position.

Probe description.- The gas sampling probe, shown in figure 3, was a boundary-layer survey-type pitot tube. The probe tip was mounted in a 7.94-millimeter-diameter supporting tube with enough offset for actuator rod clearance. The probe-actuating mechanism provided motion for vertical traversing and yaw in the horizontal plane. The static-pressure probe was of similar design with a cone angle of 28° and four orifices located 14 probe diameters from the probe tip. Pitot pressure surveys were made with the gas-sampling probe and were limited by probe geometry to heights of 0.381 millimeter and greater above the plate surface. Probe travel was indicated by a counter and the probe position was determined from calibration by a precision dial gage. The accuracy of the probe position was ±0.127 millimeter.

Flow measurements.- Jet air and maximum tracer gas mass flow rates were measured with corner-tapped orifice meters, as indicated in figure 2. Orifice-meter upstream static pressure and pressure drop were measured by a 300-psig (2.07×10^6 N/m^2) transducer and differential pressure gage. The static temperature at the meter was assumed to be the same as tunnel stagnation temperature. Low-range tracer flow rates (2.21×10^{-5} kg/sec) and sample gas flow rates (8.17×10^{-7} kg/sec) were read directly from mass-flow-rate meters. The mass-flow-rate instrument consists of a heated conduit which constitutes the elements of a thermopile with a voltage output proportional to the cooling effect and hence the mass flow rate of the gas passing through the transducer conduit. Average discharge coefficients, based on the orifice flow measurements, for the jet nozzle were 0.991 and 0.953 for jet- to free-stream total-pressure ratios of 0.34 and 0.6, respectively.

Visual-flow study.- A single-pass schlieren system was used in this investigation to facilitate observation of the flow. Flow patterns on the plate surface were defined by streaks of an oil and lampblack mixture applied prior to a test run. The patterns were lifted from the surface by a coating of a commercially manufactured room-temperature-vulcanized (RTV) silicone rubber. The rubber was poured on the surface and cured at room temperature for approximately 1 hour. As the mixture cures, the oil is absorbed in the rubber and, as a result, leaves a permanent record of the flow pattern.

Survey Procedure

Prior to each test run, the chromatograph was calibrated with a 1-percent ethane-nitrogen mixture and checked for repeatability. After establishment of tunnel run conditions, the jet pressure was set and the tracer gas, ethane, metered to maintain an approximate 1-percent mixture. A sample of this jet mixture was withdrawn, analyzed, and the chromatograph readout signal attenuated to indicate full scale on the chart. The full-scale reading was assumed to be an indication of 100-percent jet flow and subsequent survey concentration readings were measured relative to this reference reading.

The gas concentration and pressure surveys were stepwise from the plate surface outward. A diaphragm-type vacuum pump was used to withdraw samples from regions of low pressure and the pump was bypassed when pitot pressure was above atmospheric. The sample flow was throttled, whether pumped or bypassed, to maintain a constant sample mass flow rate. While a sample was being analyzed, the probe was moved to a new position and the sample line was flushed adequately prior to introduction of a new sample. Periodically, during a test run, the jet mixture was analyzed to check the reference reading. Pitot-pressure measurements were made with the gas sample probe at each concentration measurement position. Static-pressure measurements were made at each concentration survey station and fairings of these data were used in the calculation of local Mach number. The spacing between static-pressure data points on a vertical survey was approximately 0.635 millimeter.

Data Processing

Pressure survey data were reduced to determine local values of Mach number, mass flow per unit area, and corrected pitot pressure at each survey station. Since the mixture of jet gas and tunnel air is essentially air in air, no correction was necessary for the mixture ratio of specific heats γ_{mix}. Mach numbers were determined from the Rayleigh pitot formula and a mass-weighted average of tunnel and jet stagnation temperatures was used in the calculation of local mass flow per unit area.

Flow Model

A schematic of an envisioned flow field about an underexpanded jet issuing perpendicular to a supersonic primary stream is presented in figure 4. Similar flow models are presented in references 1 to 4. The obstruction created by the jet flow into the primary stream forms a primary bow shock wave upstream of the jet. As the bow wave impinges on the boundary layer, it creates an adverse pressure gradient which tends to separate the flow from the wall. The inner jet flow expands, is recompressed by the jet shock, and approximates the pressure of the external flow at the jet boundary. Immediately downstream of the jet, the flow is highly expanded to a value less than free-stream pressure and is recompressed further downstream.

DISCUSSION AND RESULTS

Model Surface Pressures

Axial static-pressure distributions along the model surface center line are presented in figure 5 for a range of jet- to free-stream total-pressure ratios of 0.3 to 1.0. Wall pressure, normalized by free-stream stagnation pressure, is given as a function of axial position. The influence of jet pressure on wall static pressure can be seen in the separation region associated with the jet bow wave, the region of high expansion at the downstream station of 5.9 jet diameters, and the rise to ambient pressure at $x/D \geq 45$. Measurements at the positions of $x/D = -30.93$ and 91 were constant over the range of pressure ratios. Similar results of flat-plate pressure distributions are reported in reference 5.

Lateral distributions obtained from cross plots of plate static pressure are shown in figure 6. Symmetry about the longitudinal center line was assumed and wall pressure ratio is plotted as a function of lateral position at survey stations of 7, 15, and 30 jet diameters and total-pressure ratios of 0.34 and 0.6. The validity of the symmetry assumption appears to be substantiated by the oil-streak flow pattern shown in the photograph of figure 7. The detached bow wave of the jet was estimated, by the method of reference 8, to be located at a value of $x/D = -0.8$. The body assumed for this calculation was a cylinder normal to the free stream with a diameter equal to that of the jet orifice. A region of reversed flow ahead of the jet is indicated by the upstream flow of oil to approximately 5 jet diameters. It is felt that the indicated streamline seen at this position represents a boundary of the separation region rather than of the bow wave. At a distance of approximately 5 diameters downstream of the jet, a similar boundary forms on either side of the longitudinal center line.

Mach number distribution.- The local Mach number profiles of figure 8 were cross-plotted and are presented in figure 9 in the form of contour plots. In general, the contours

exhibit symmetry about the plane $y/D = 0$ with a more rapid approach to free-stream Mach number for the lower jet pressure cases.

Concentration measurements.- Results of the injected gas concentration data are presented in figures 10 to 12. Concentration profiles and jet bow shock waves in the x, z plane are shown in figure 10(a) for jet- to free-stream total-pressure ratios of 0.34 and 0.6. Bow-wave locations at the three axial survey stations were determined by pressure surveys and are in close agreement with schlieren measurements. The injected gas penetration height h is defined as the vertical distance above the model surface at which the mass fraction K is equal to zero. The expected greater penetration occurs at the higher jet pressure for the three survey stations. At an x/D of 7 and 15, penetration is increased 41 percent by the jet total-pressure increase of 76 percent. At the 30-diameter station, an increase of 22 percent in penetration was measured for the same pressure increase. In the case of total-pressure ratio of 0.34, the penetration height decreases from a value of 6.6 jet diameters at $x/D = 7$ to 6.0 at $x/D = 15$ and increases to a value of 6.2 at an axial position of 30 diameters. For the higher pressure ratio of 0.6, the penetration height decreases with increasing x/D to h/D values of 9.2, 8.5, and 7.5 at stations of 7, 15, and 30 diameters, respectively. Penetration, measured in terms of position of maximum concentration, can be seen in figure 10(a) to increase with x/D for a pressure ratio of 0.34 and reach a peak value of 4.54 jet diameters at $x/D = 15$ for $p_{t,j}/p_{t,\infty} = 0.6$.

Profiles of concentration in planes of constant y/D are presented in figures 10(b) and 10(c). Cross plots of these data are shown in figure 11 as a function of lateral position y/D and constant values of vertical distance z/D. The curves of figures 10 and 11 were used to generate the contour maps of figure 12.

The contours, presented in figure 12, represent lines of constant mass-fraction concentration of the injected gas in the y, z plane at the three downstream survey stations. The contours, in general, exhibit symmetry about the x, z plane with the exception of the case of $x/D = 7$ and $p_{t,j}/p_{t,\infty} = 0.6$. The Mach number contours (fig. 9) are indicative of symmetric pressure distributions for this case and differences in test conditions are considered to be negligible for the runs made for this configuration. The reason for this nonuniformity of concentration is not known. Examination of the contours of figure 12 shows that maximum vertical penetration occurs in off-axis positions except for the $p_{t,j}/p_{t,\infty} = 0.6$ and $x/D = 7$ and 15 configurations. At the pressure ratio of 0.6, the maximum values of jet penetration were approximately 9.2, 8.5, and 8 jet diameters at axial stations of 7, 15, and 30 diameters, respectively. At the lower pressure ratio of 0.34, the maximum penetration was approximately a constant value of 7 diameters at each station.

Penetration, measured in terms of cross-sectional area containing the injected gas, is highest at the 7-diameter station and is approximately constant at the two stations further downstream for both pressure ratios. The effect of increasing jet pressure is a substantial increase (40 percent) in penetration area at each survey station.

Combustion limits of H_2-air.- The chromatography measurement, a volumetric concentration and therefore a molecule count, can be converted to a mass fraction by

$$K = \frac{m_{j,x}}{m_{mix}} = B\frac{\mathcal{M}_j}{\mathcal{M}_{mix}} \tag{1}$$

Since the injected gas mixture for this investigation is essentially a binary one of air in air, the volumetric and gravimetric concentrations are essentially equal. The limits of flammability of a hydrogen-air mixture are approximately 4 and 75 percent by volume (ref. 9). The degree of similarity in mixing and penetration for different gases is not fully understood at the present time. If the curves of figure 12 are assumed to simulate the volumetric concentration distribution of hydrogen in air, the contour line $K = 0.04$ represents the lower combustion limit and $K = 0.3$, a stoichiometric fuel-air mixture. The maximum value of concentration measured during these tests was 56 percent which is well below the upper limit of 75 percent. Integration of the contour plots shows that cross-sectional area containing a combustible mixture decreases slightly with downstream distance for both test pressure ratios. This area was approximately 65 percent of the area under the $K = 0$ contour for all test configurations and the area inside the stoichiometric contour ($K = 0.3$) decreases with downstream distance and decreasing pressure ratio.

Mass flow per unit area.- The pressure and concentration data were reduced to local values of mass flow per unit area and cross plots of the profiles were used to generate the contours of figure 13. The contours represent lines of constant injected gas mass flow per unit area at the survey station. These values are nondimensionalized by the maximum local mass-flow value for each test configuration. Integration of these plots indicates maximum inaccuracies of ±20 percent of the metered jet flow over the range of test configurations, the error becoming more negative with increasing axial survey position. It was noted in the discussion of the concentration contours that the area under the $K = 0$ curve decreases with axial position increase. To maintain mass continuity, a proportional increase in mass flow per unit area is required.

Comparison with existing data.- The choice of a correlating parameter for jet penetration has yet to be firmly established. However, an empirical equation given in reference 6 is

$$\frac{h}{D} = 1.68\left(\frac{\rho_j V_j^2}{\rho_\infty V_\infty^2}\cos^2\theta\,\frac{M_\infty}{M_j}\right)^{0.5}\left(\frac{x}{D}\right)^{0.0866} \tag{2}$$

where the $\cos\theta$ provides that the normal component of jet momentum flux be used in the case of angled injection. Injectant molecular weight and specific heat ratio were varied in the experiments of references 5 and 6 and the effects on penetration were reported to be negligible. The results of the tests of reference 5 also indicate that penetration is independent of the boundary-layer state. The boundary-layer thickness was not varied during the present investigation and a search of the literature indicates no existing data relevant to the influence of this parameter on penetration. One might expect the boundary-layer thickness and extent of the separation region relative to the jet diameter to exert some influence on the penetration, but experimental data would be necessary to verify this effect.

The penetration data of the present report and those of references 5 and 6 are shown in figure 14. Figure 14(a) shows penetration to be a very weak function of axial position at the lower momentum ratios and indicates a stronger dependence as momentum ratio is increased. The plot of penetration as a function of momentum ratio in figure 14(b) shows h/D varying approximately as the square root of jet- to free-stream momentum ratio.

CONCLUDING REMARKS

The data obtained from this experiment indicate that the chromatograph technique is a satisfactory method for making concentration measurements of a secondary jet. The results of the data obtained show that penetration height and cross-sectional area containing the injected gas decrease slightly with increasing axial position and increase with jet momentum flux. Although the range of variables (two momentum ratios and three axial positions) is not sufficient to formulate a correlating expression, comparison with existing data indicates that penetration is directly proportional to approximately the square root of jet- to free-stream momentum ratio and is a weak function of axial position.

Langley Research Center,
National Aeronautics and Space Administration,
Langley Station, Hampton, Va., October 31, 1966,
124-10-02-04-23.

REFERENCES

1. Charwat, A. F.; and Allegre, J.: Interaction of a Supersonic Stream and a Transverse Supersonic Jet. AIAA J., vol. 2, no. 11, Nov. 1964, pp. 1965-1972.

2. Vinson, P. W.: Prediction of Reaction Control Effectiveness at Supersonic and Hypersonic Speeds. Rept. OR 6487, U.S. Army Missile Command (Redstone Arsenal, Ala.), Mar. 1965.

3. Janos, Joseph J.: Loads Induced on a Flat-Plate Wing by an Air Jet Exhausting Perpendicularly Through the Wing and Normal to a Free-Stream Flow of Mach Number 2.0. NASA TN D-649, 1961.

4. Szpiro, Edward J.: Secondary Fluid Injection Into a Supersonic Airstream. Rept. No. 65-2, Mech. Eng. Res. Lab., McGill Univ., Apr. 1965.

5. Zukoski, Edward E.; and Spaid, Frank W.: Secondary Injection of Gases Into a Supersonic Flow. Preprint 64-110, Am. Inst. Aeronaut., Astronaut., Jan. 1964.

6. Vranos, Alexander; and Nolan, James J.: Supersonic Mixing of Helium and Air. Bumblebee Rept. TG-63-53, Appl. Phys. Lab., Johns Hopkins Univ., June 1964, pp. 131-161.

7. Jeffrey, P. G.; and Kipping, P. J.: Gas Analysis by Gas Chromatography. The Macmillan Co., c.1964.

8. Moeckel, W. E.: Approximate Method for Predicting Form and Location of Detached Shock Waves Ahead of Plane or Axially Symmetric Bodies. NACA TN 1921, 1949.

9. Lewis, Bernard; and von Elbe, Guenther: Combustion, Flames and Explosions of Gases. Second ed., Academic Press, Inc. (New York), 1961.

Table I. - PLATE STATIC PRESSURE ORIFICE LOCATION

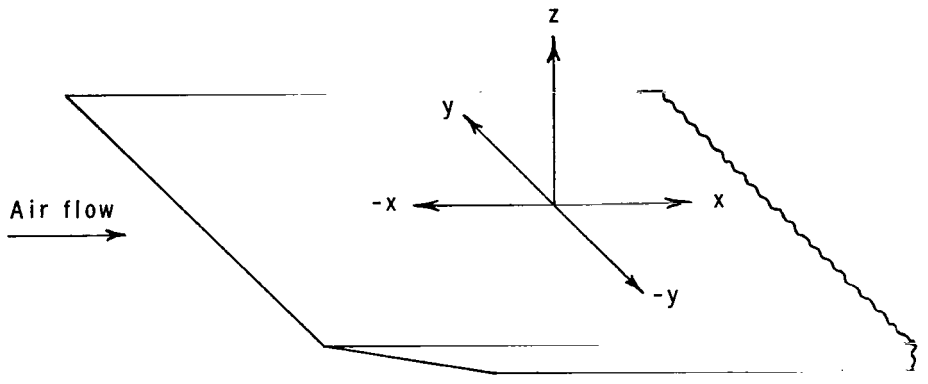

Orifice number	x/D	y/D
1	-30.93	0
2	-20.62	0
3	- 5.79	0
4	0	-5.79
5	5.79	0
6	0	5.79
7	0	-20.62
8	0	-41.24
9	0	-61.86
10	0	30.93
11	0	51.55
12	0	72.17
13	15.79	-24.29
14	26.50	-11.79
15	28.25	-6.52
16	28.99	0
17	28.78	3.28
18	27.49	9.20
19	22.02	18.83
20	32.62	-50.25
21	44.45	0
22	45.55	38.89
23	49.50	-76.17
24	54.72	-24.37
25	58.35	-13.48
26	59.92	0
27	59.49	6.78
28	56.78	19.01

Orifice number	x/D	y/D
29	69.07	58.97
30	75.38	0
31	82.99	-36.95
32	88.52	-20.43
33	90.85	0
34	90.27	10.29
35	86.13	28.83
36	92.58	79.07
37	106.31	0
38	111.24	-49.53
39	118.72	-27.38
40	121.78	0
41	120.83	13.77
42	115.47	38.66
43	137.24	0
44	139.51	-62.13
45	148.87	-34.33
46	152.70	0
47	151.76	17.28
48	144.75	48.48
49	168.17	0
50	167.74	-74.70
51	178.97	-41.30
52	183.63	0
53	182.48	20.78
54	174.13	58.29
55	199.10	0
56	209.08	-48.25
57	203.41	68.08

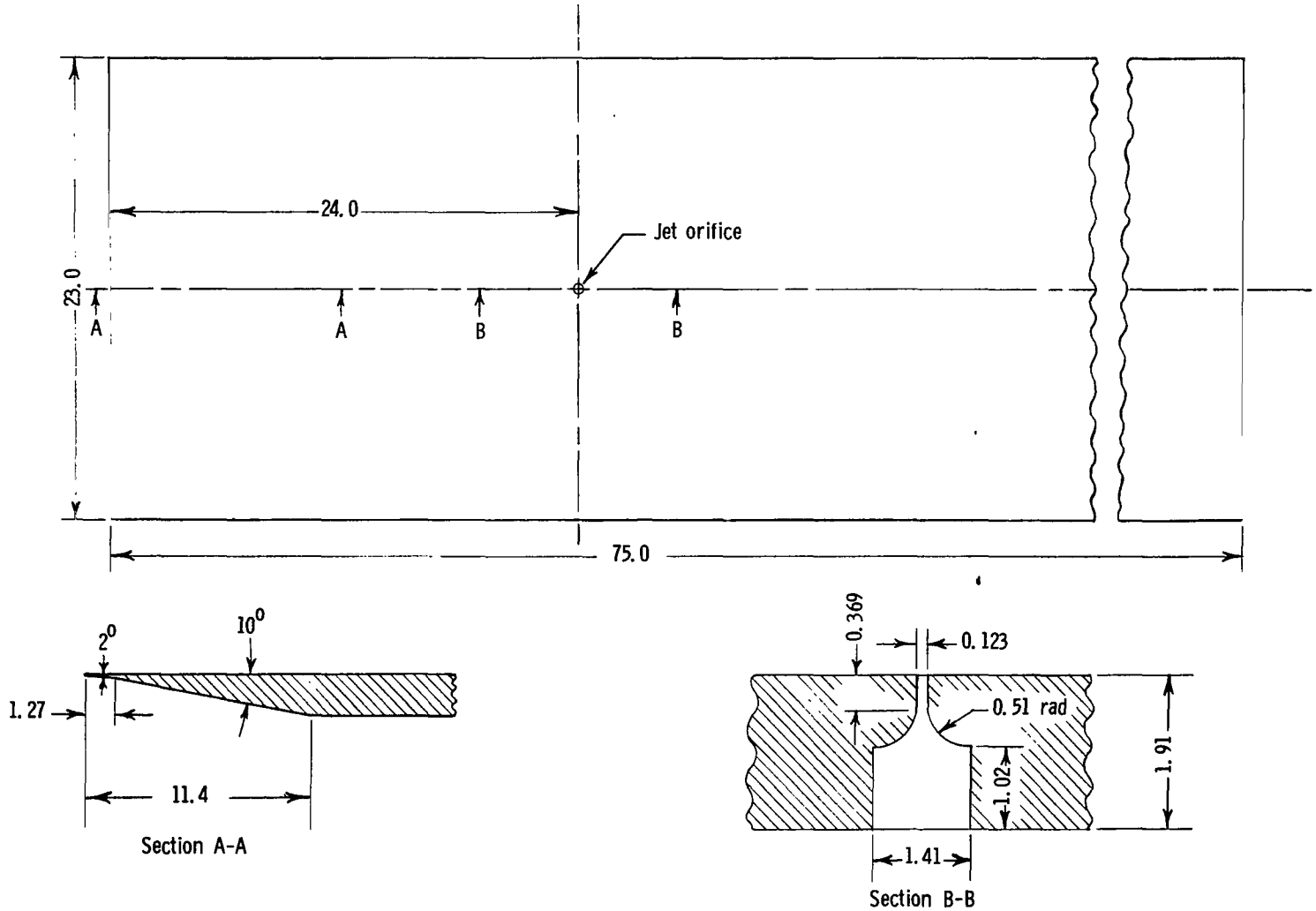

Figure 1.- Sketch of model. All dimensions are in centimeters.

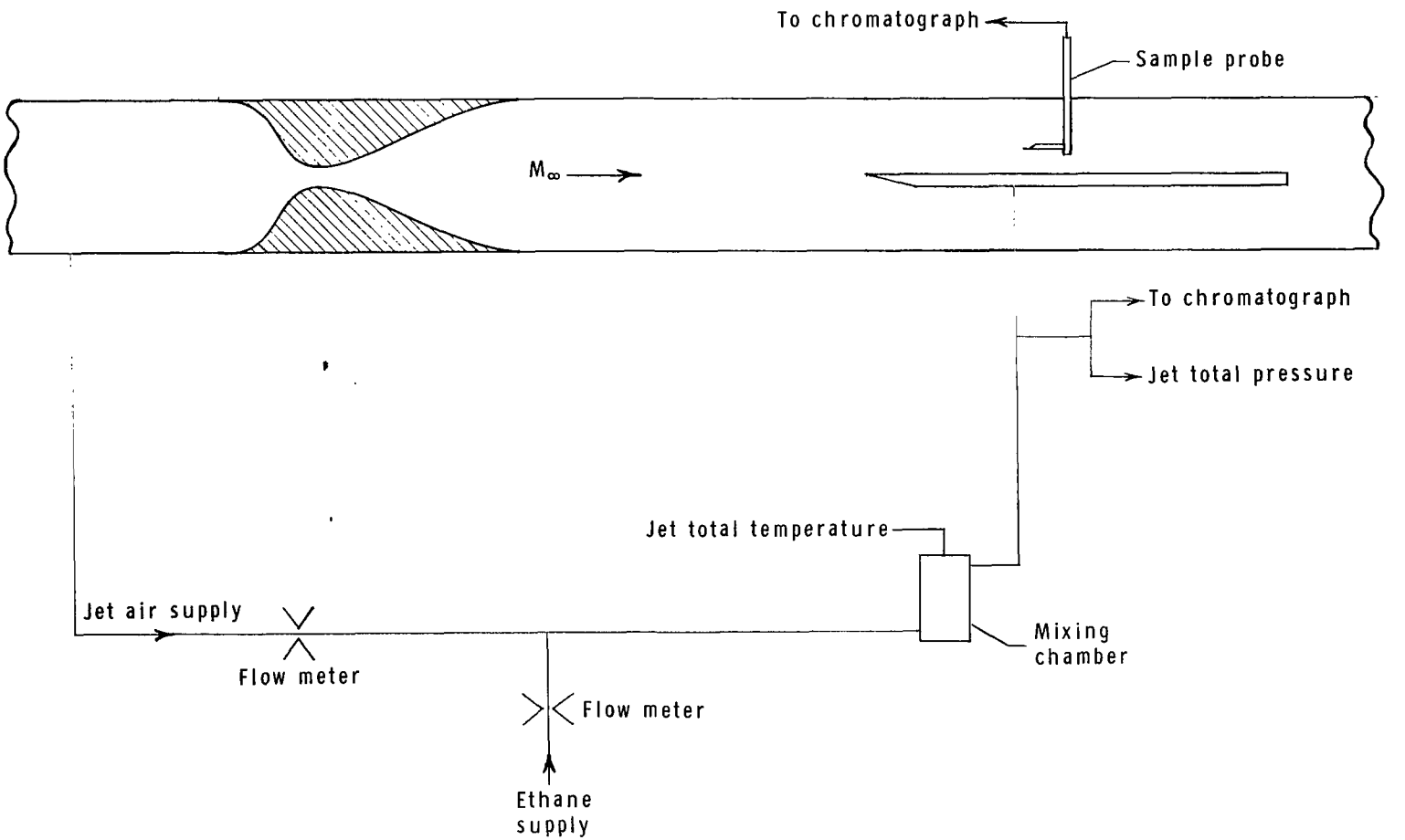

Figure 2.- Tunnel and secondary flow schematic.

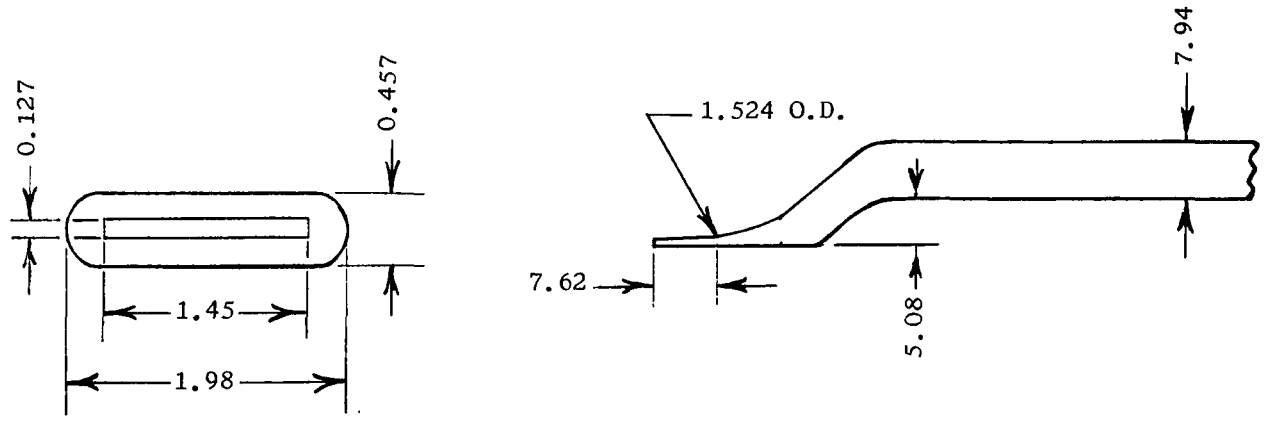

Gas-sampling probe

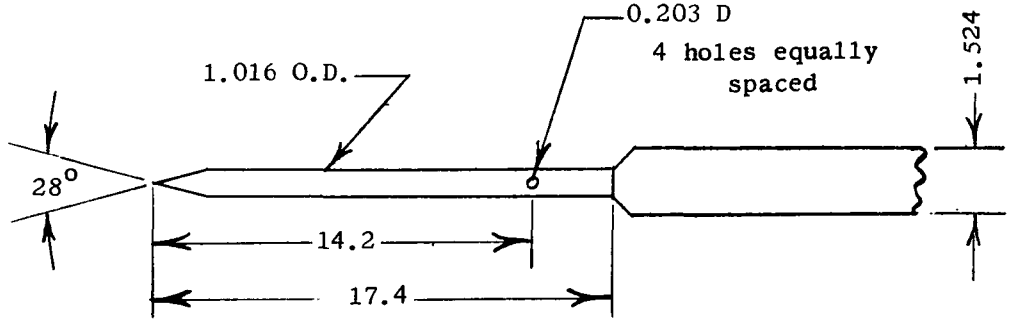

Static-pressure probe

Figure 3.- Survey-probe design. All dimensions are in millimeters.

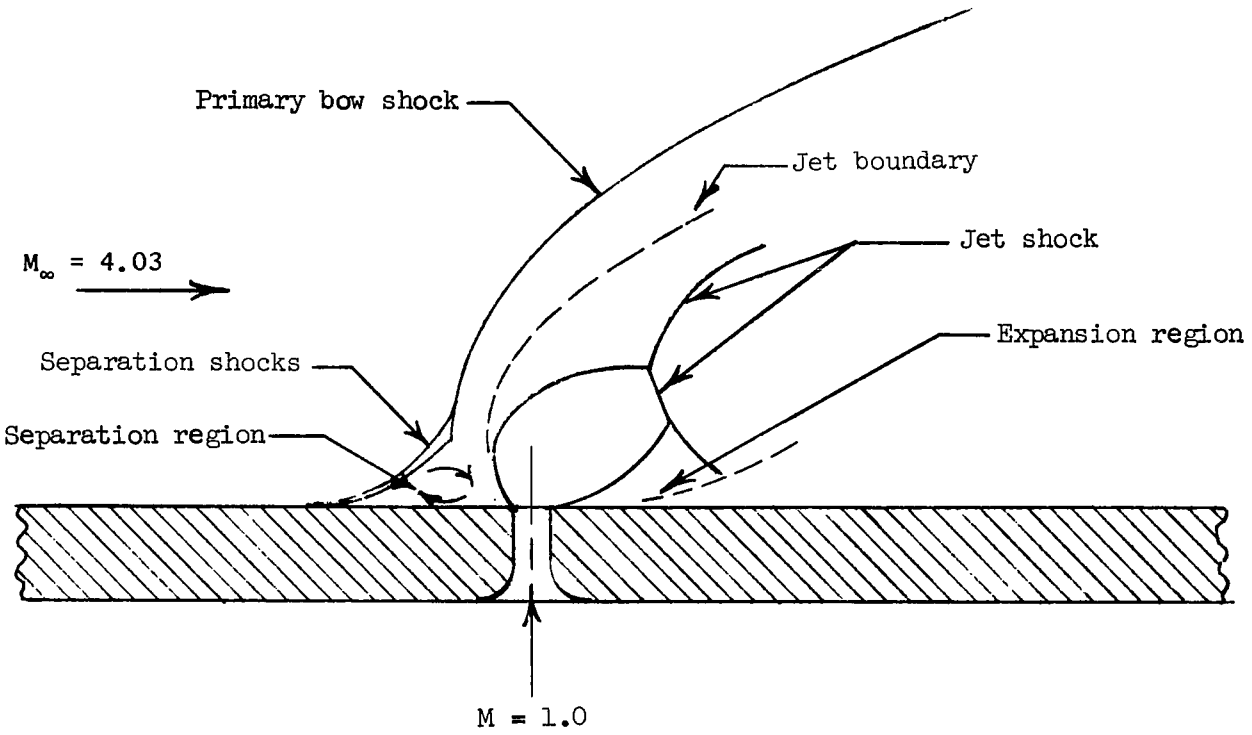

Figure 4.- Schematic of flow field about jet.

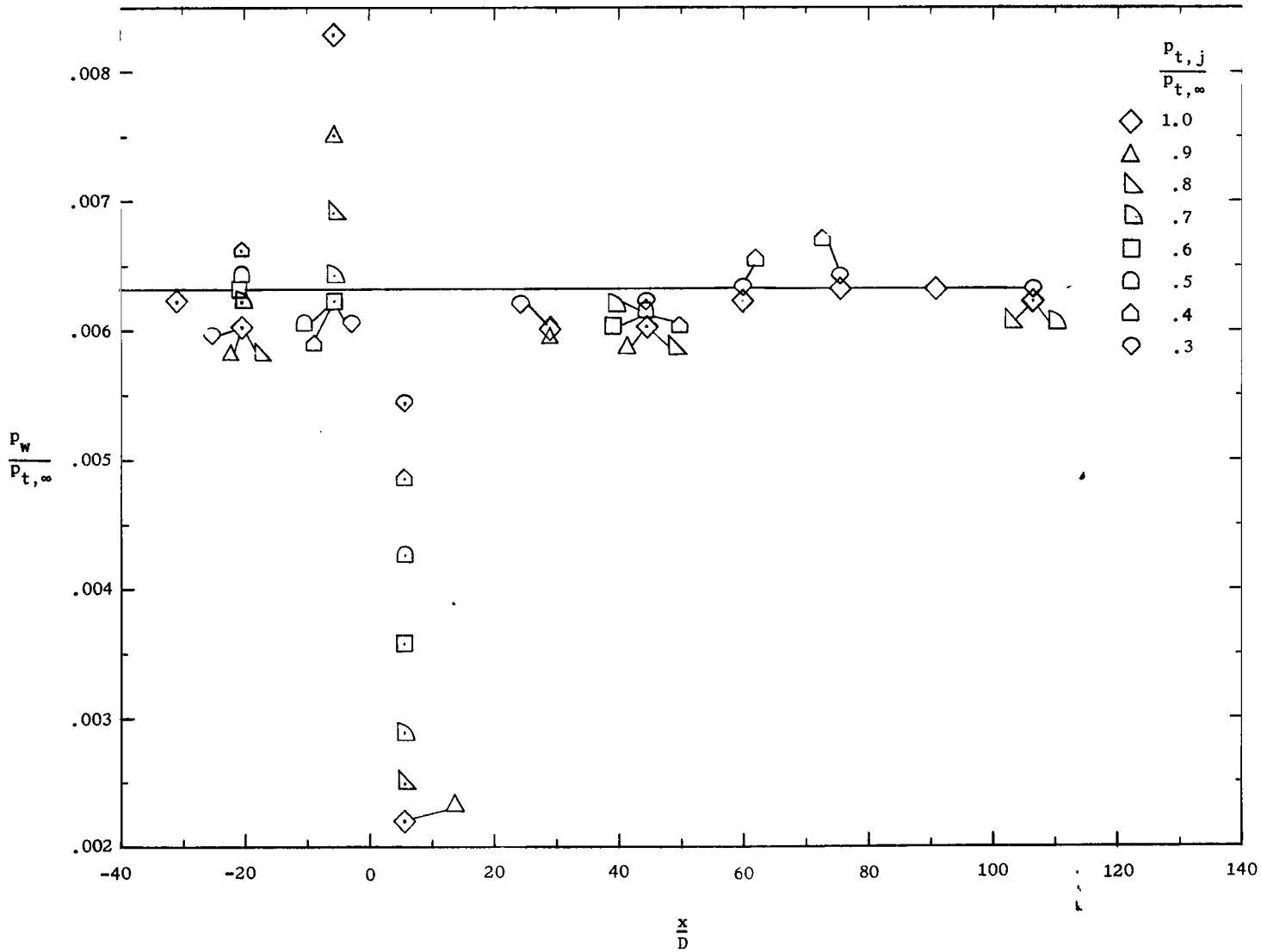

Figure 5.- Axial-plate static-pressure distribution.

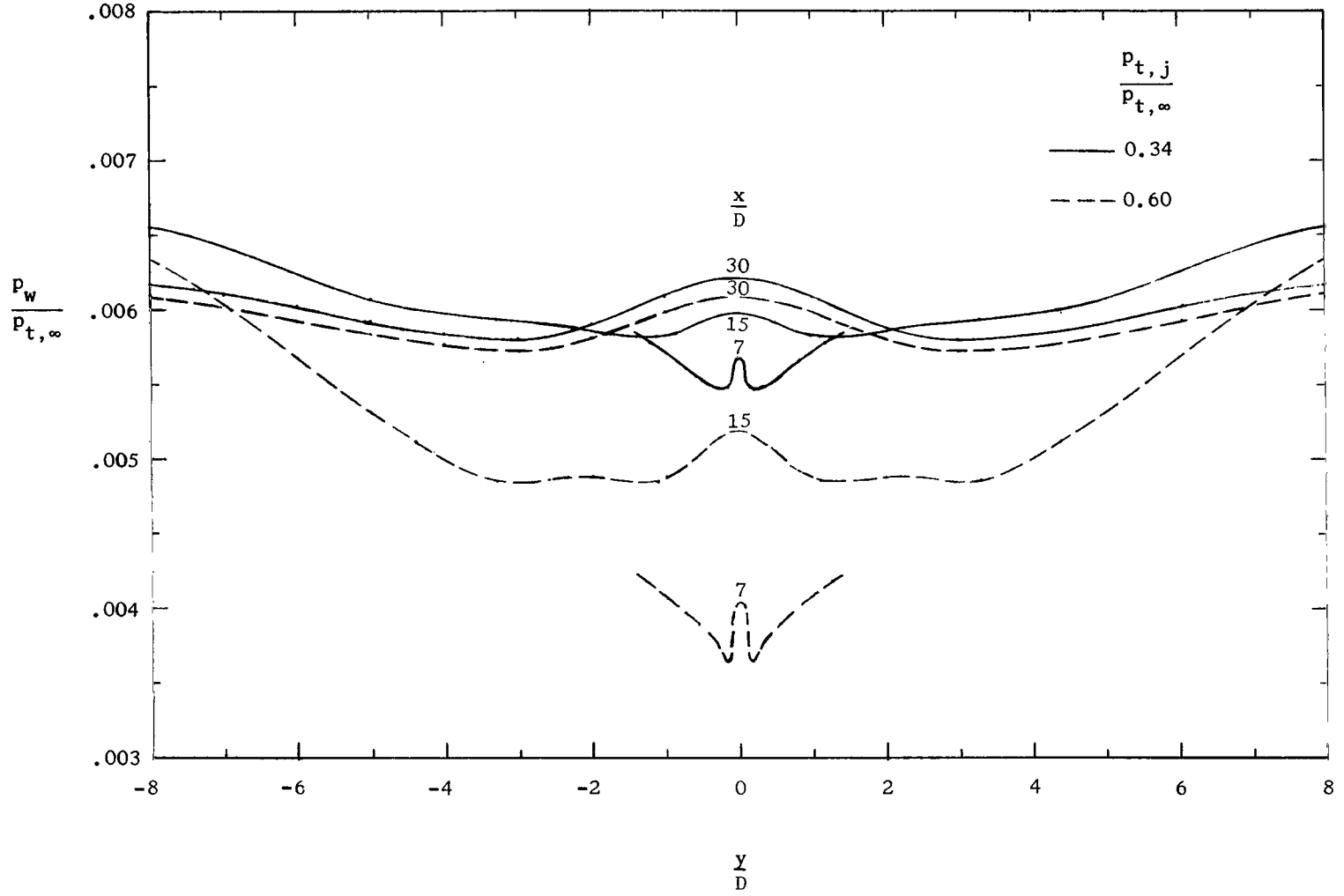

Figure 6.- Lateral-plate static-pressure distribution.

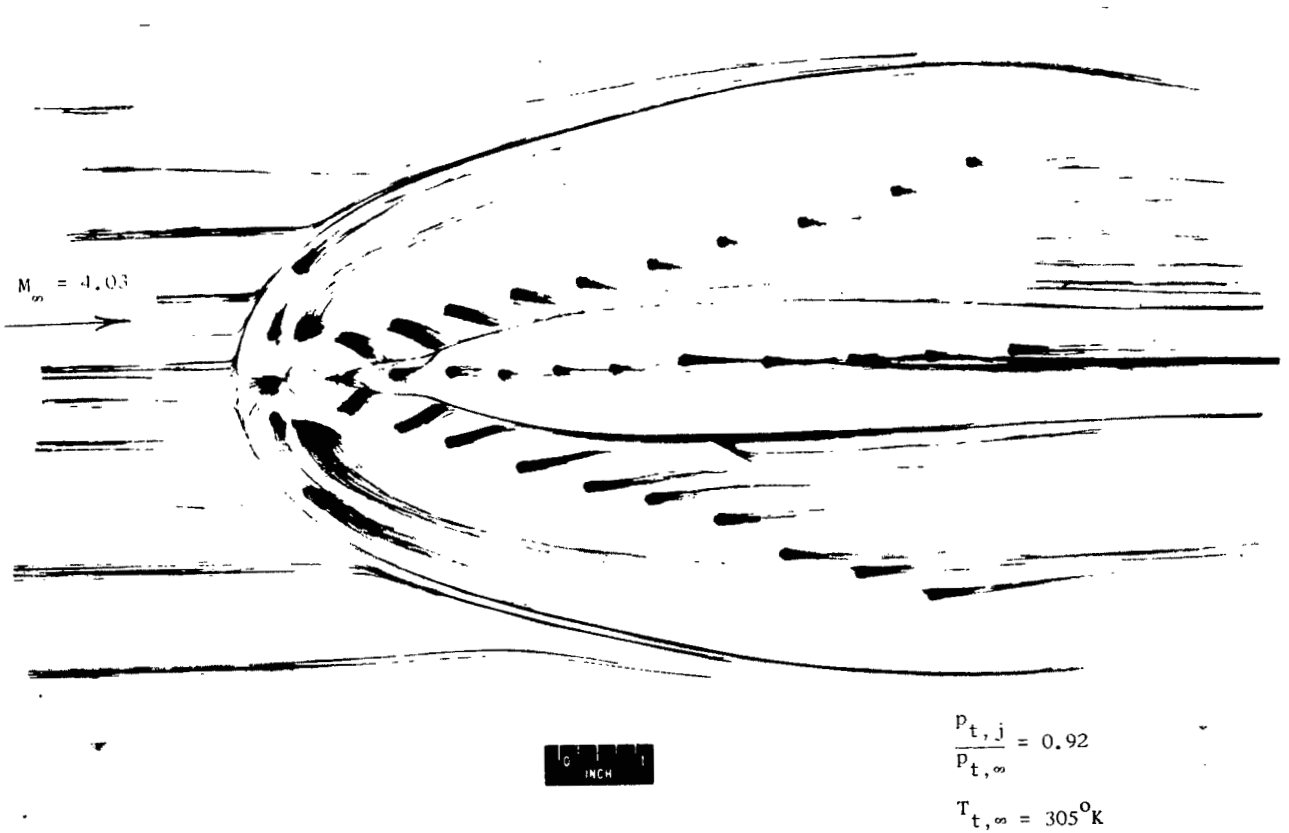

Figure 7.- Surface flow pattern.

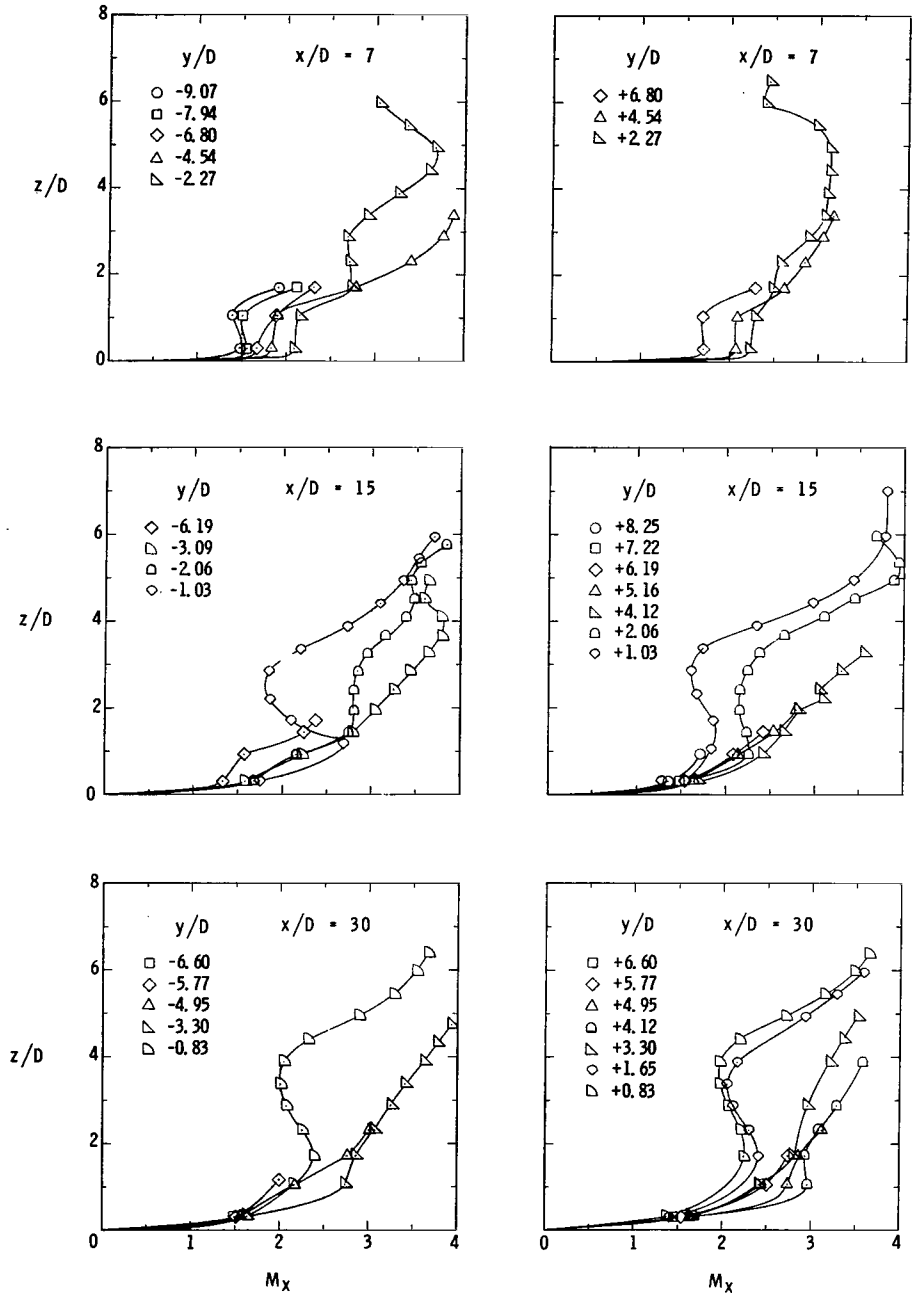

(a) $p_{t,j}/p_{t,\infty} = 0.34$.

Figure 8.- Mach number profiles.

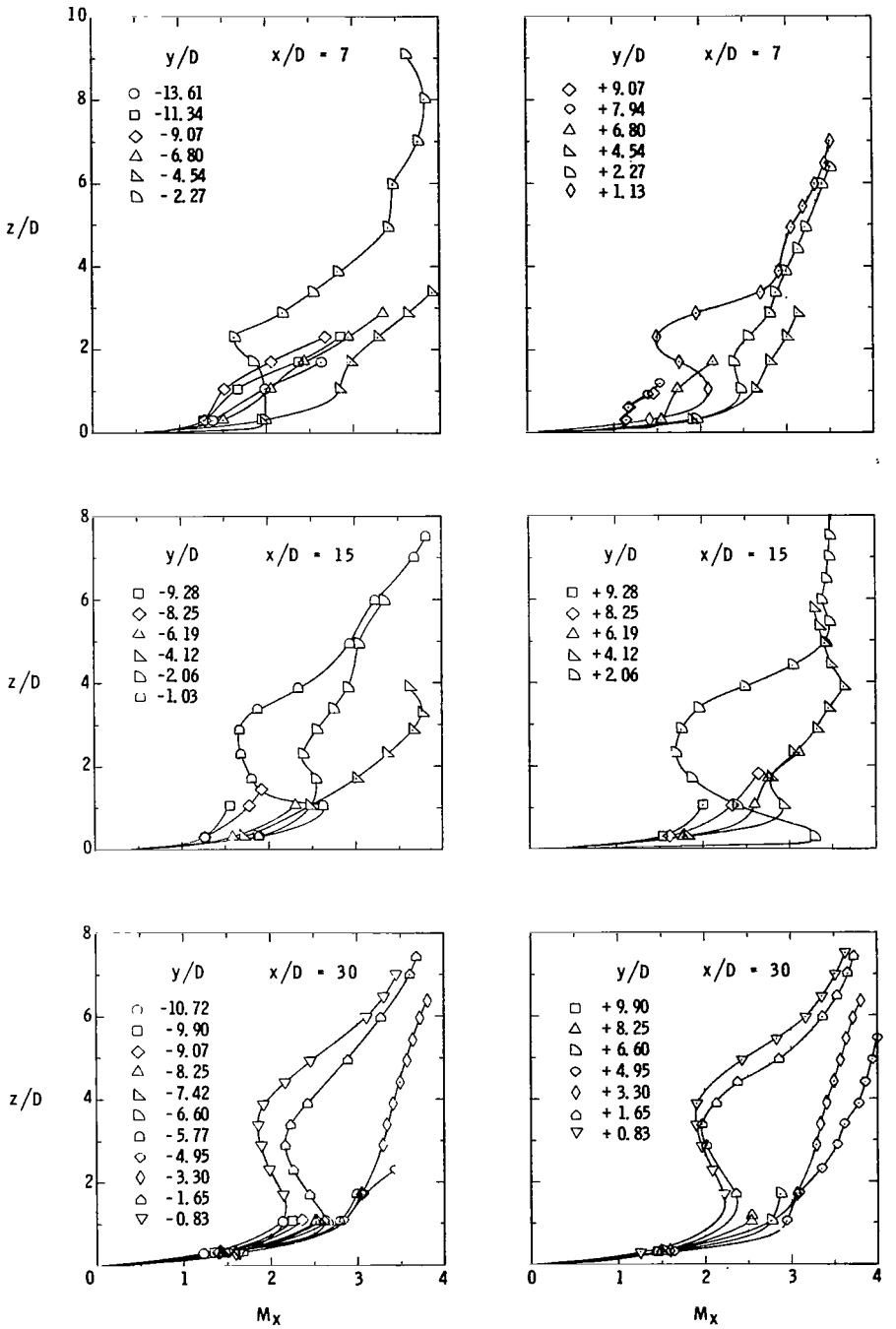

(b) $p_{t,j}/p_{t,\infty} = 0.60$.

Figure 8.- Concluded.

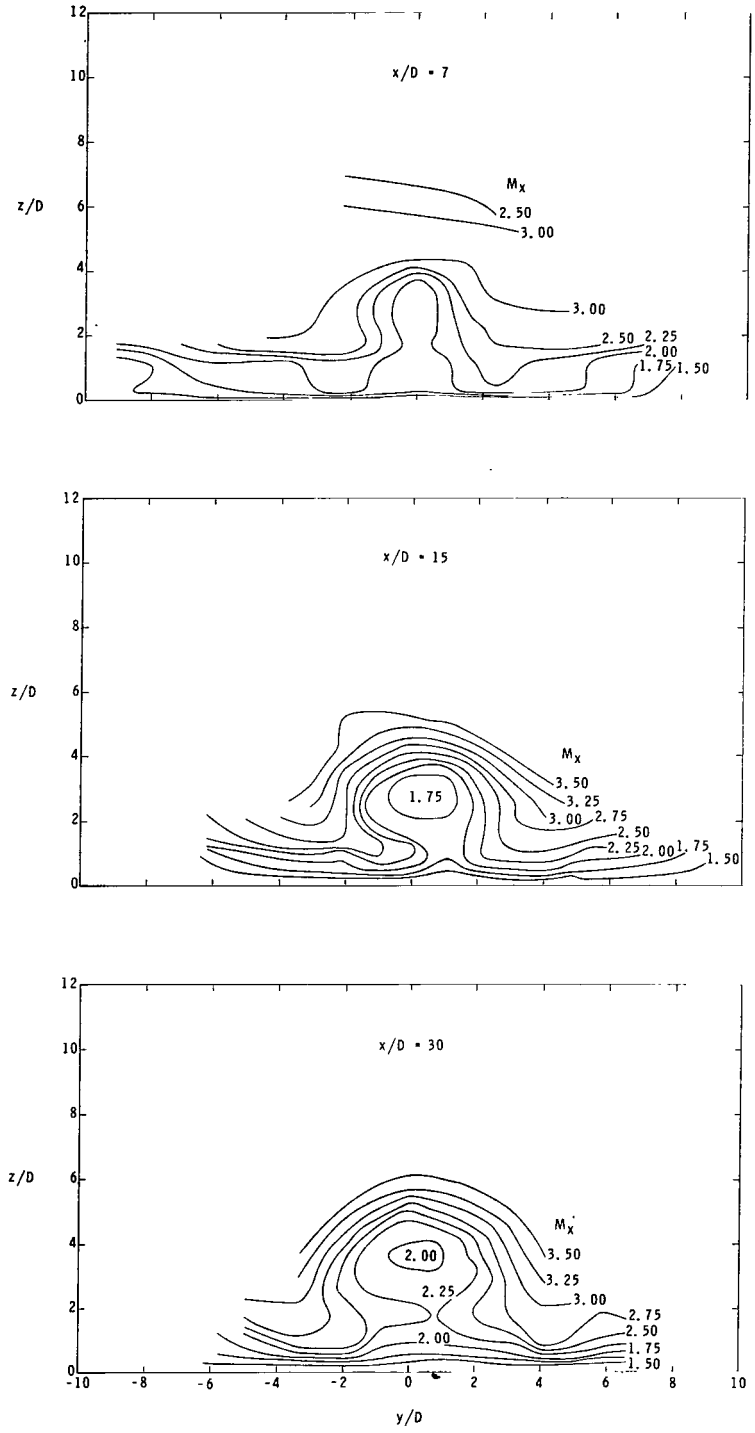

(a) $p_{t,j}/p_{t,\infty} = 0.34$.

Figure 9.- Mach number contours.

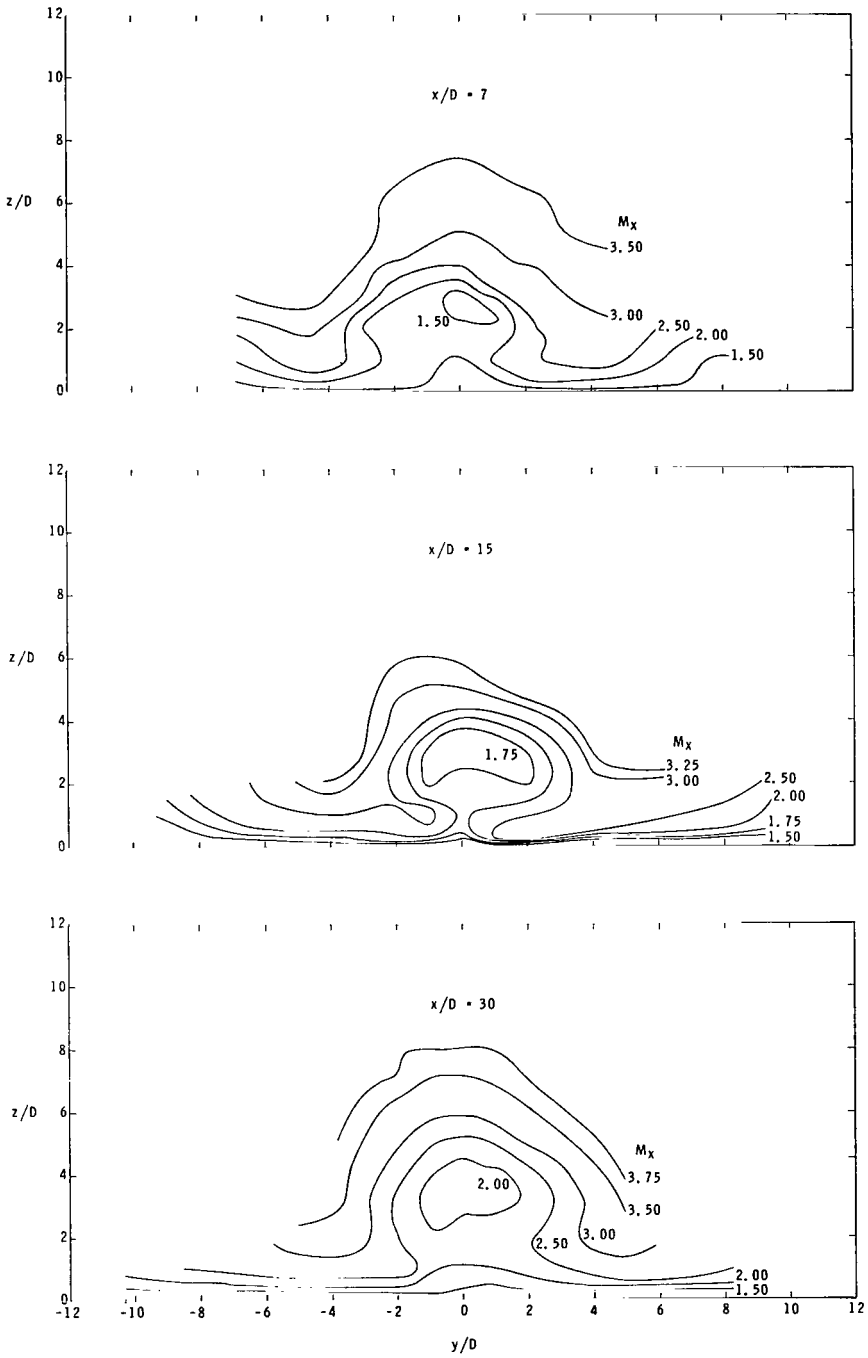

(b) $p_{t,j}/p_{t,\infty} = 0.60$.

Figure 9.- Concluded.

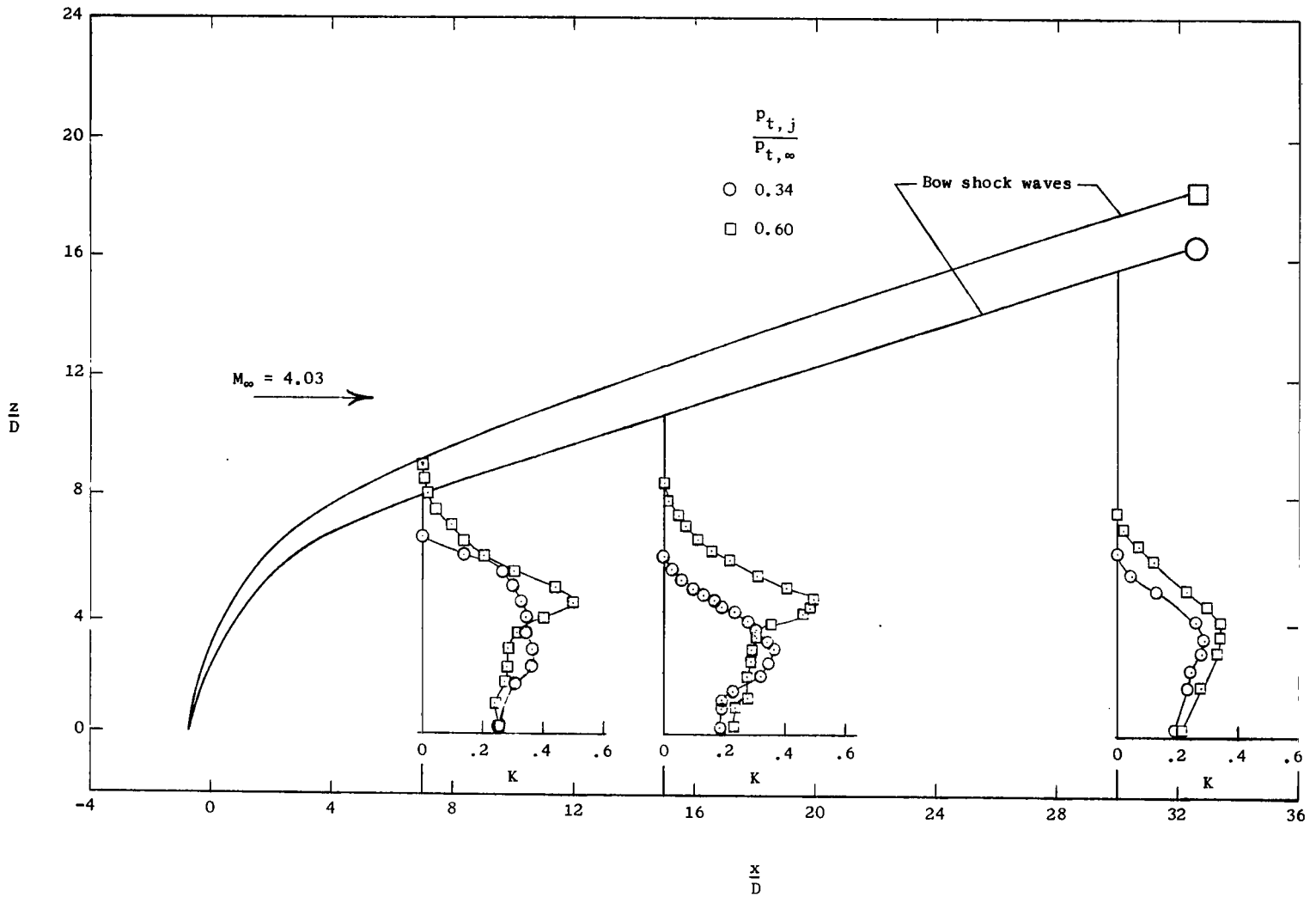

(a) Axial center-line profiles.

Figure 10.- Concentration profiles.

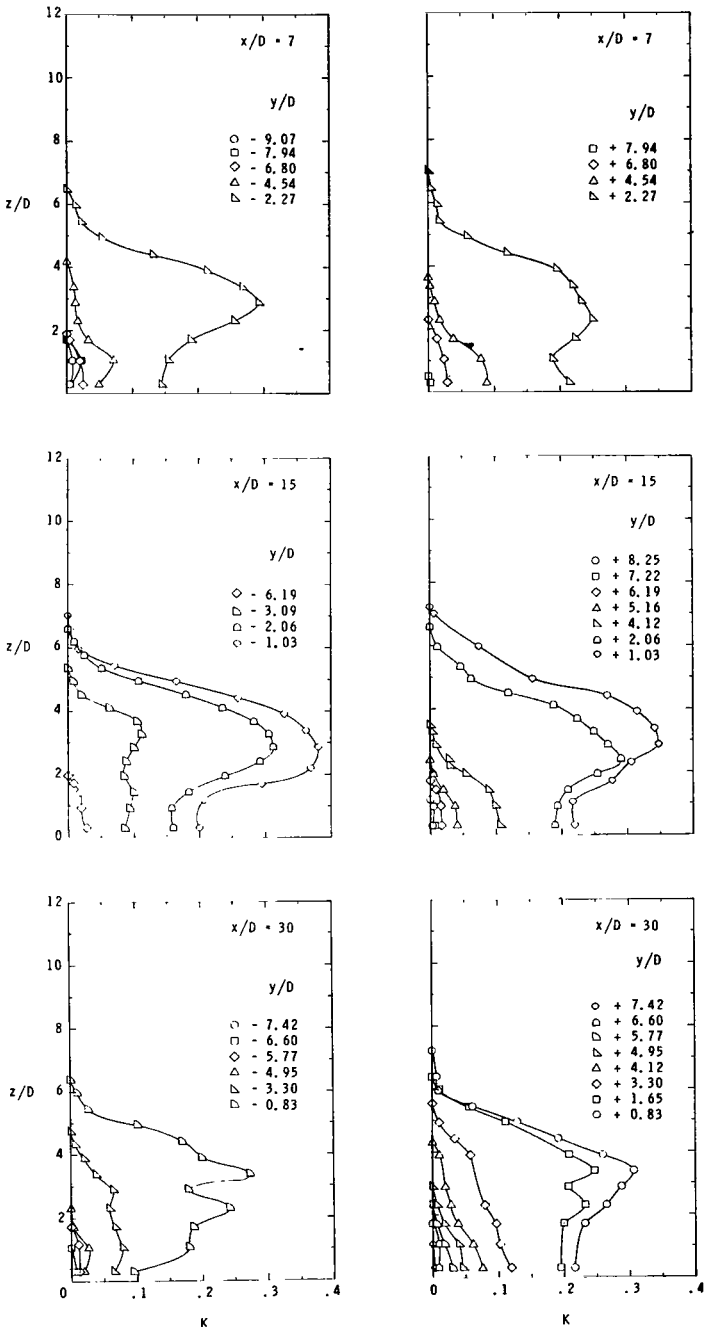

(b) Off-axis profiles; $p_{t,j}/p_{t,\infty} = 0.34$.

Figure 10.- Continued.

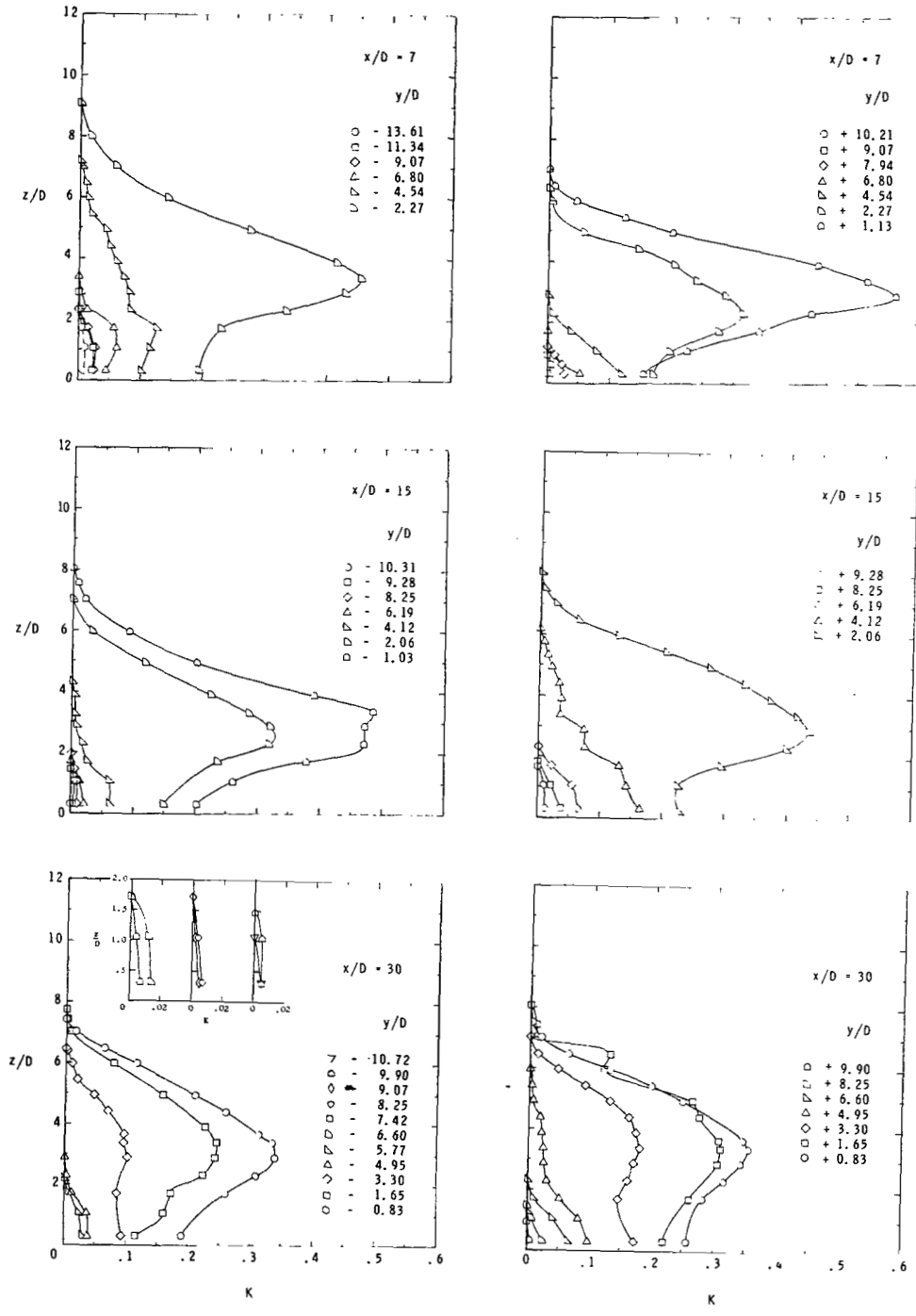

(c) Off-axis profiles; $p_{t,j}/p_{t,\infty} = 0.60$.

Figure 10.- Concluded.

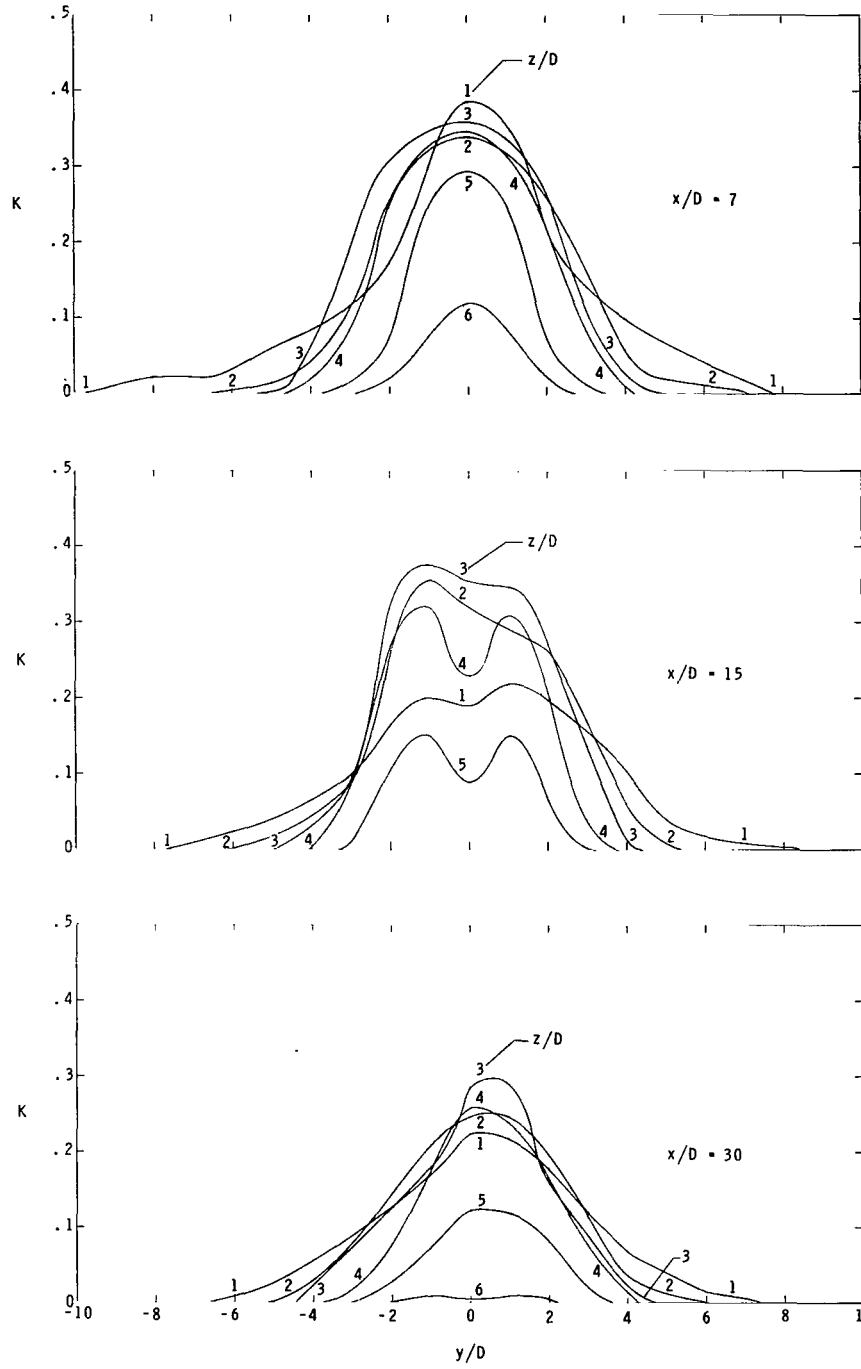

(a) $p_{t,j}/p_{t,\infty} = 0.34$.

Figure 11.- Lateral concentration distribution.

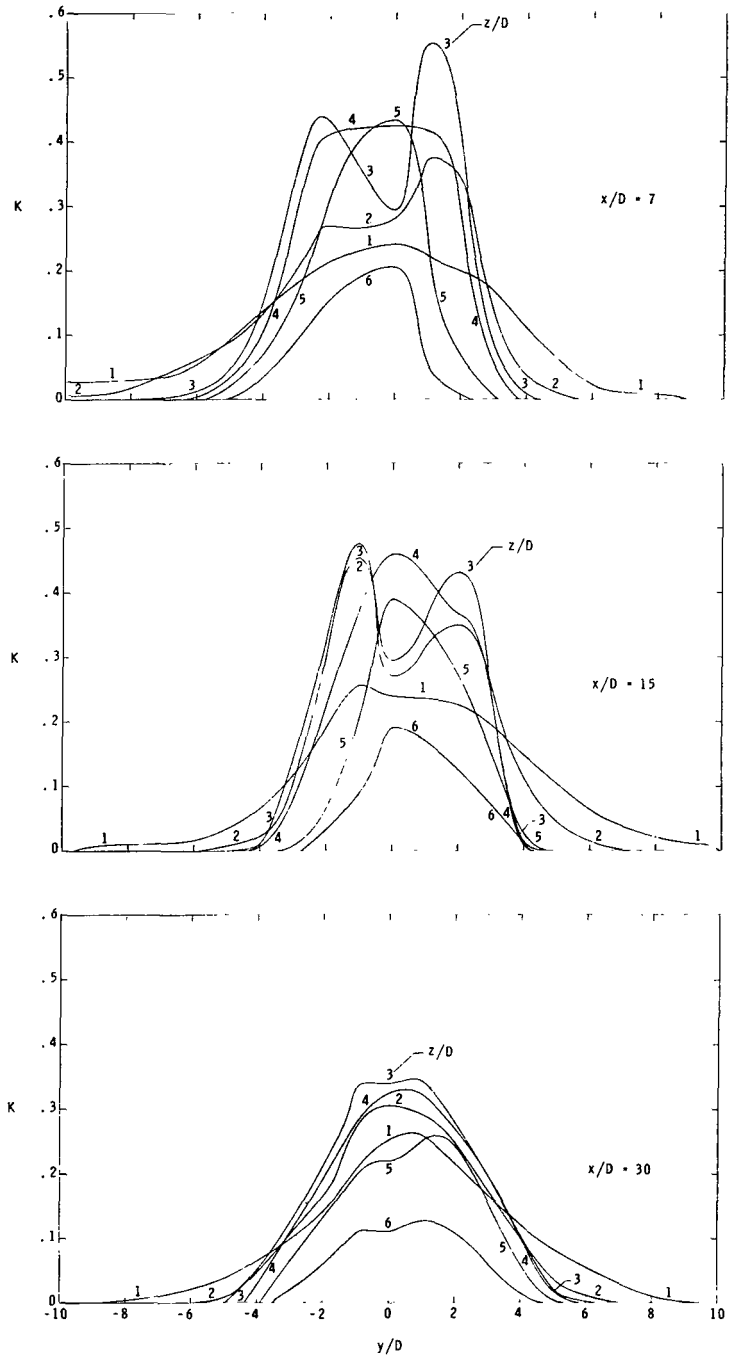

(b) $p_{t,j}/p_{t,\infty} = 0.60$.

Figure 11.- Concluded.

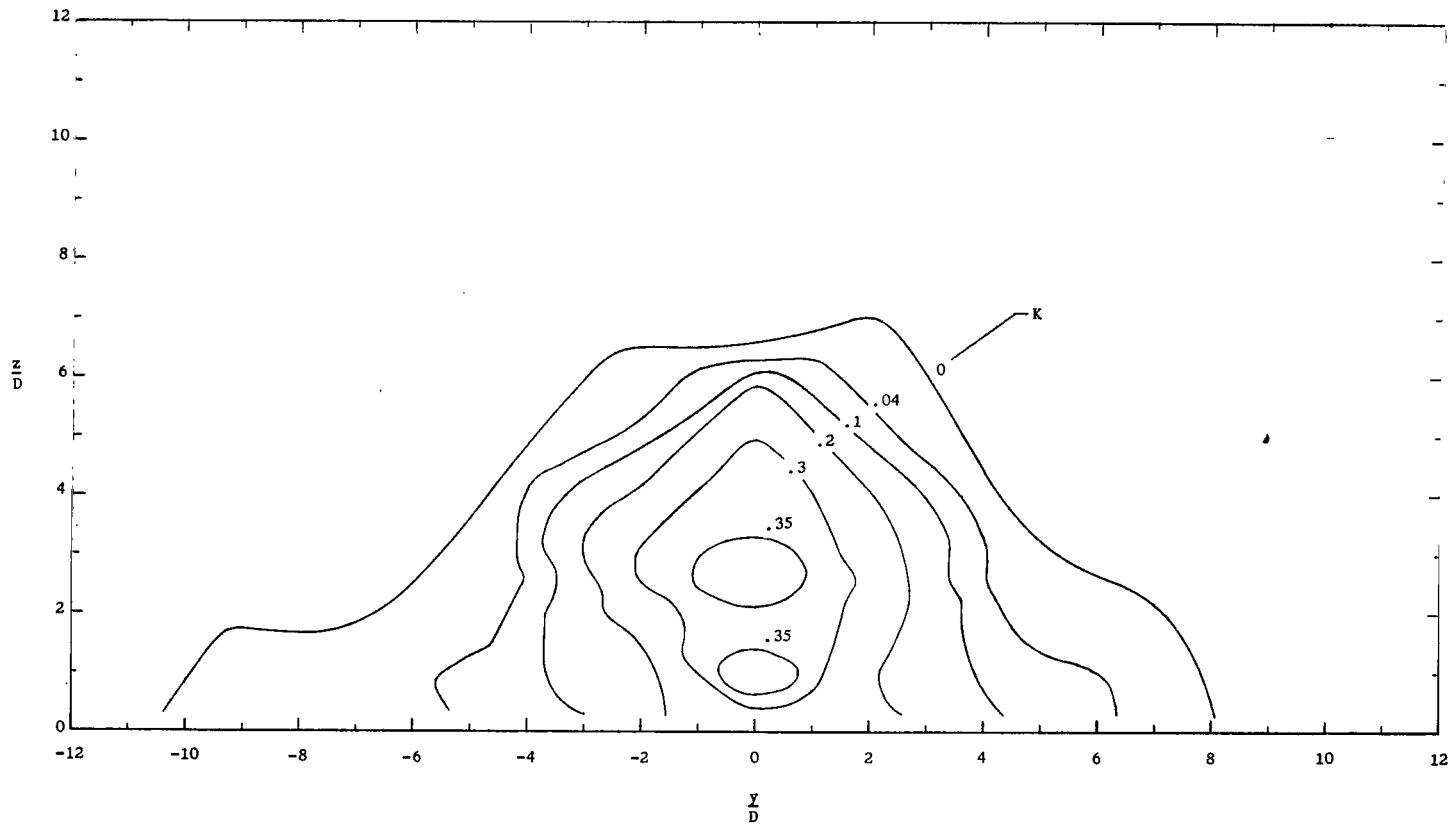

(a) x/D = 7; $p_{t,j}/p_{t,\infty} = 0.34$.

Figure 12.- Concentration contours.

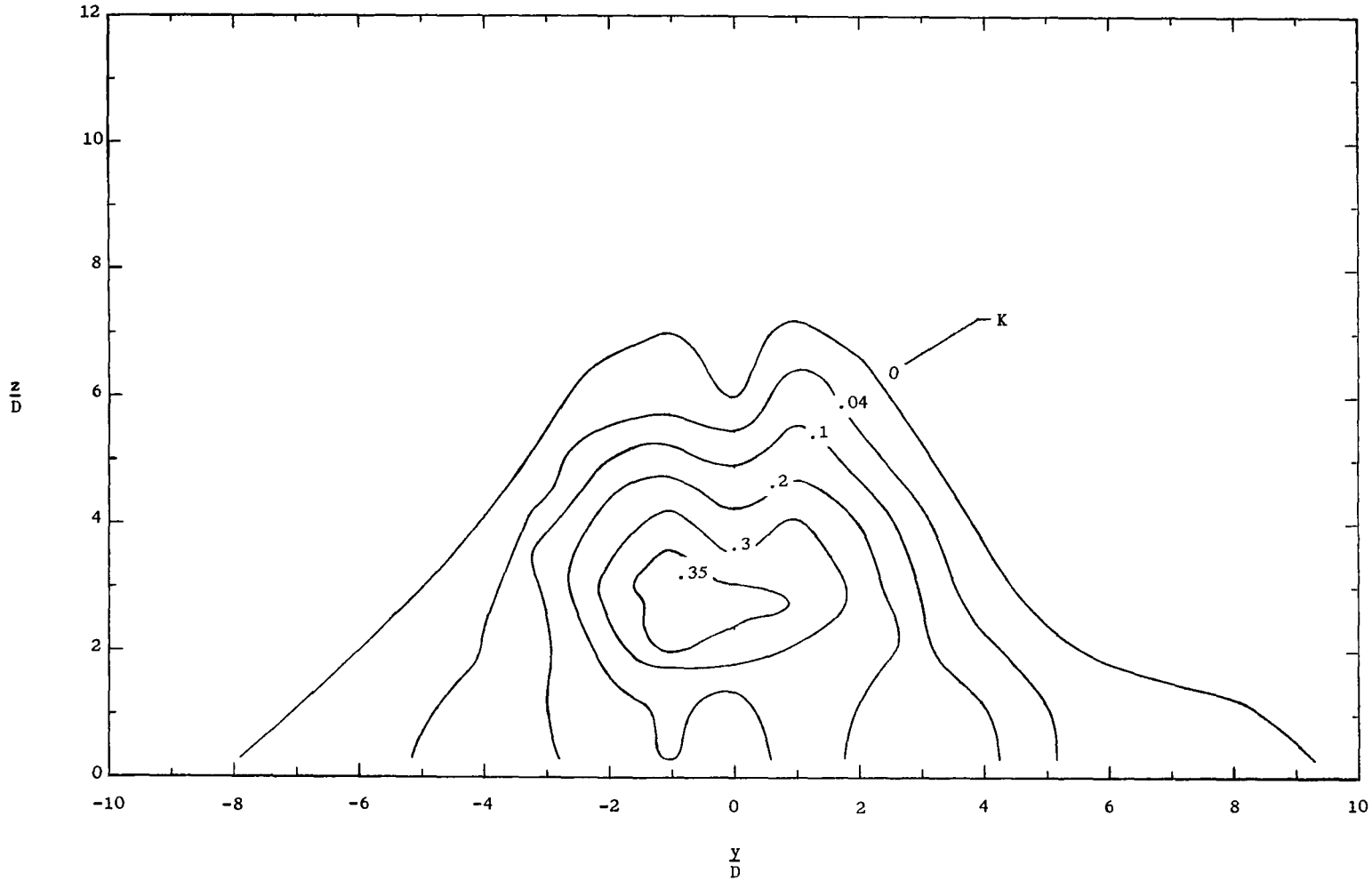

(b) x/D = 15; $p_{t,j}/p_{t,\infty}$ = 0.34.

Figure 12.- Continued.

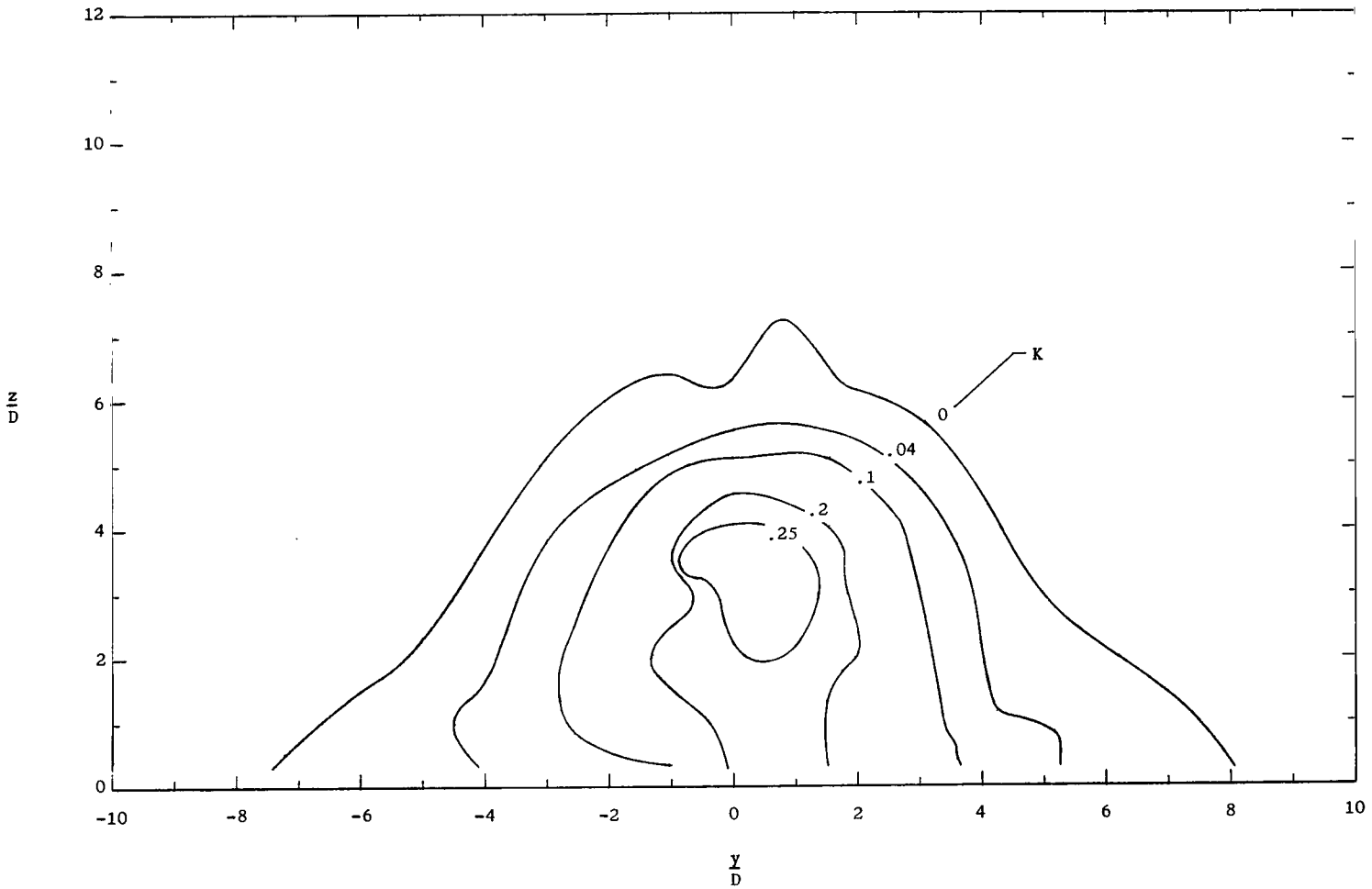

(c) $x/D = 30$; $p_{t,j}/p_{t,\infty} = 0.34$.

Figure 12.- Continued.

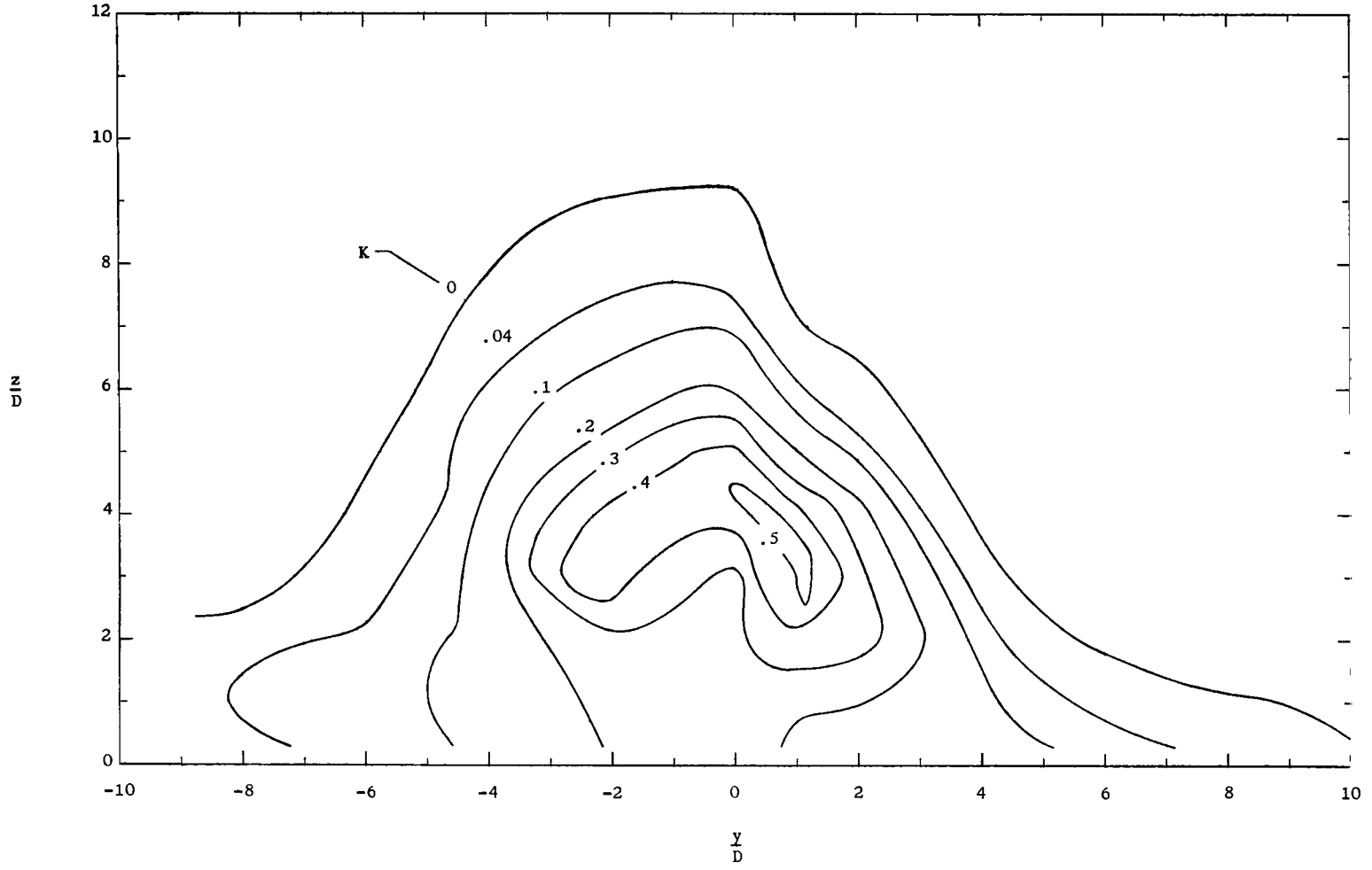

(d) x/D = 7; $p_{t,j}/p_{t,\infty} = 0.60$.

Figure 12.- Continued.

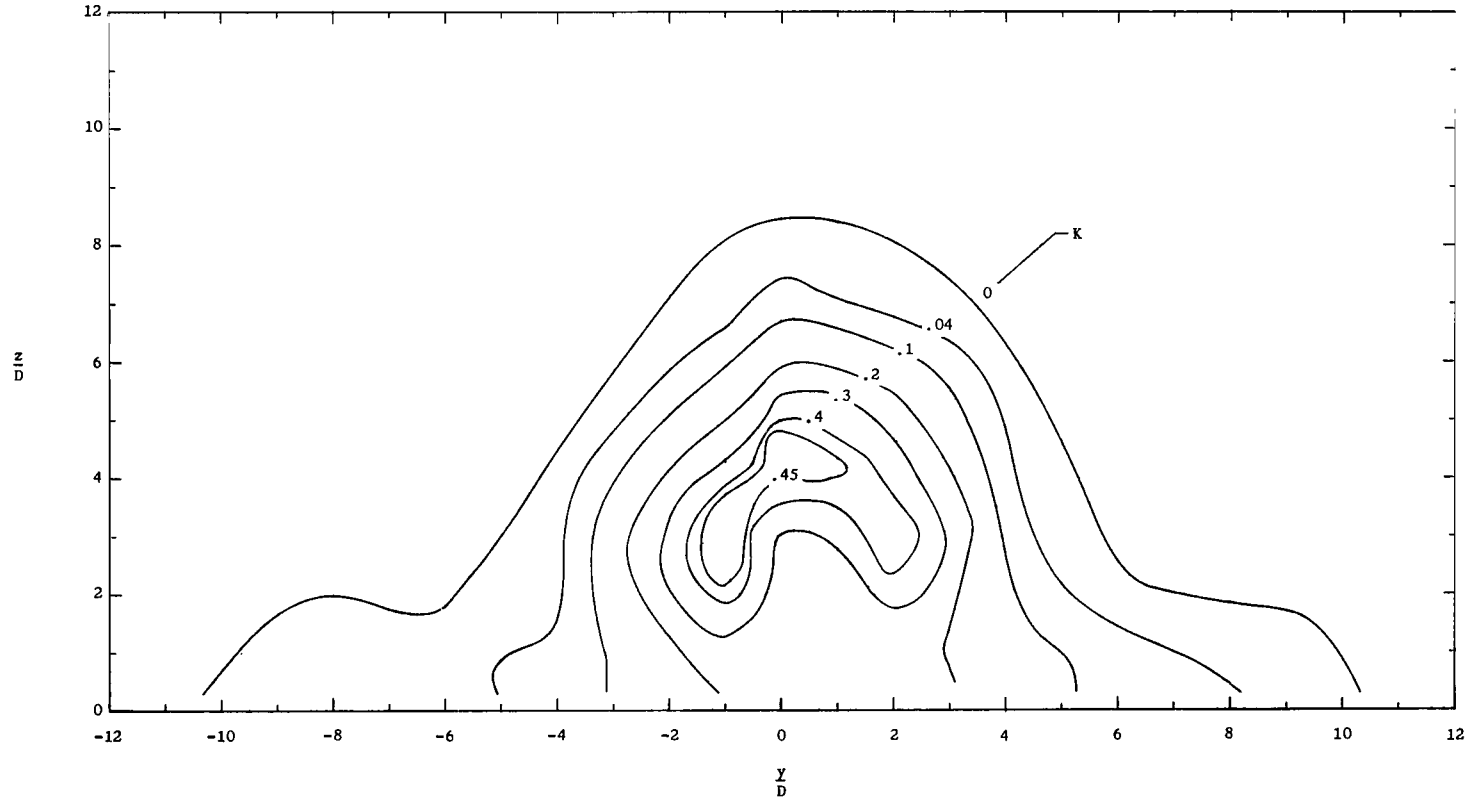

(e) x/D = 15; $p_{t,j}/p_{t,\infty} = 0.60$.

Figure 12.- Continued.

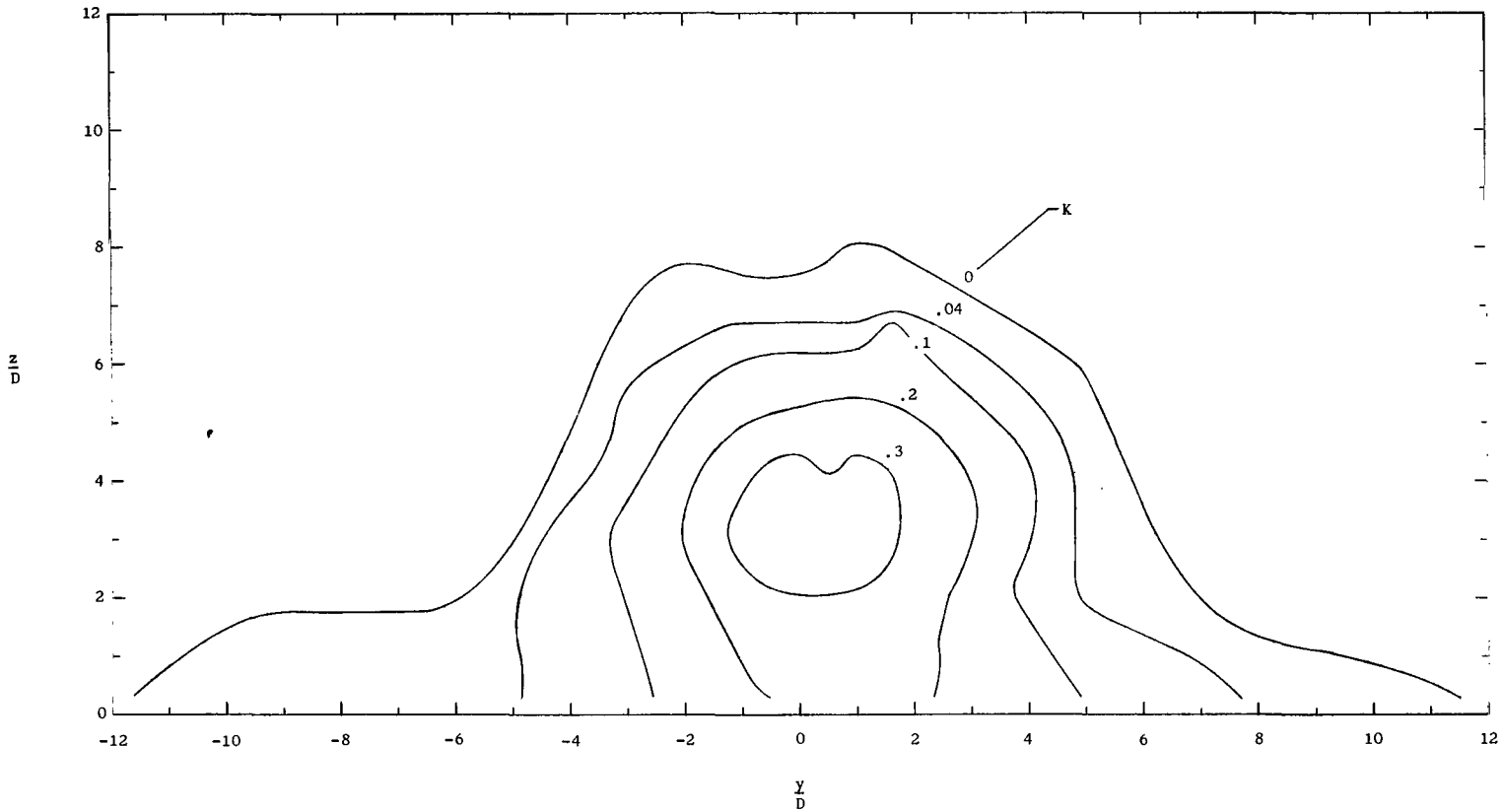

(f) x/D = 30; $p_{t,j}/p_{t,\infty} = 0.60$.

Figure 12.- Concluded.

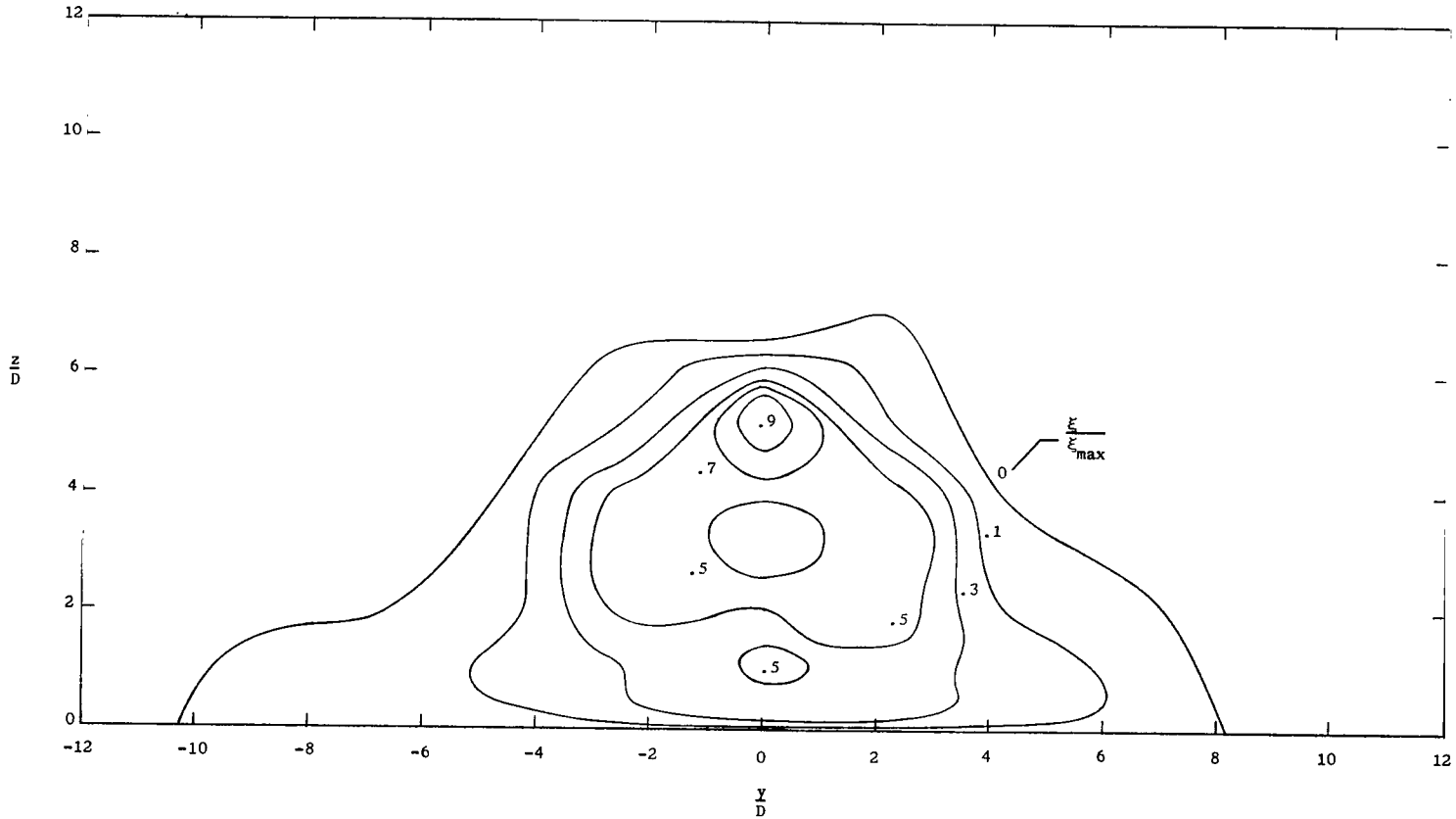

(a) x/D = 7; $p_{t,j}/p_{t,\infty} = 0.34$.

Figure 13.- Mass flow per unit area contours.

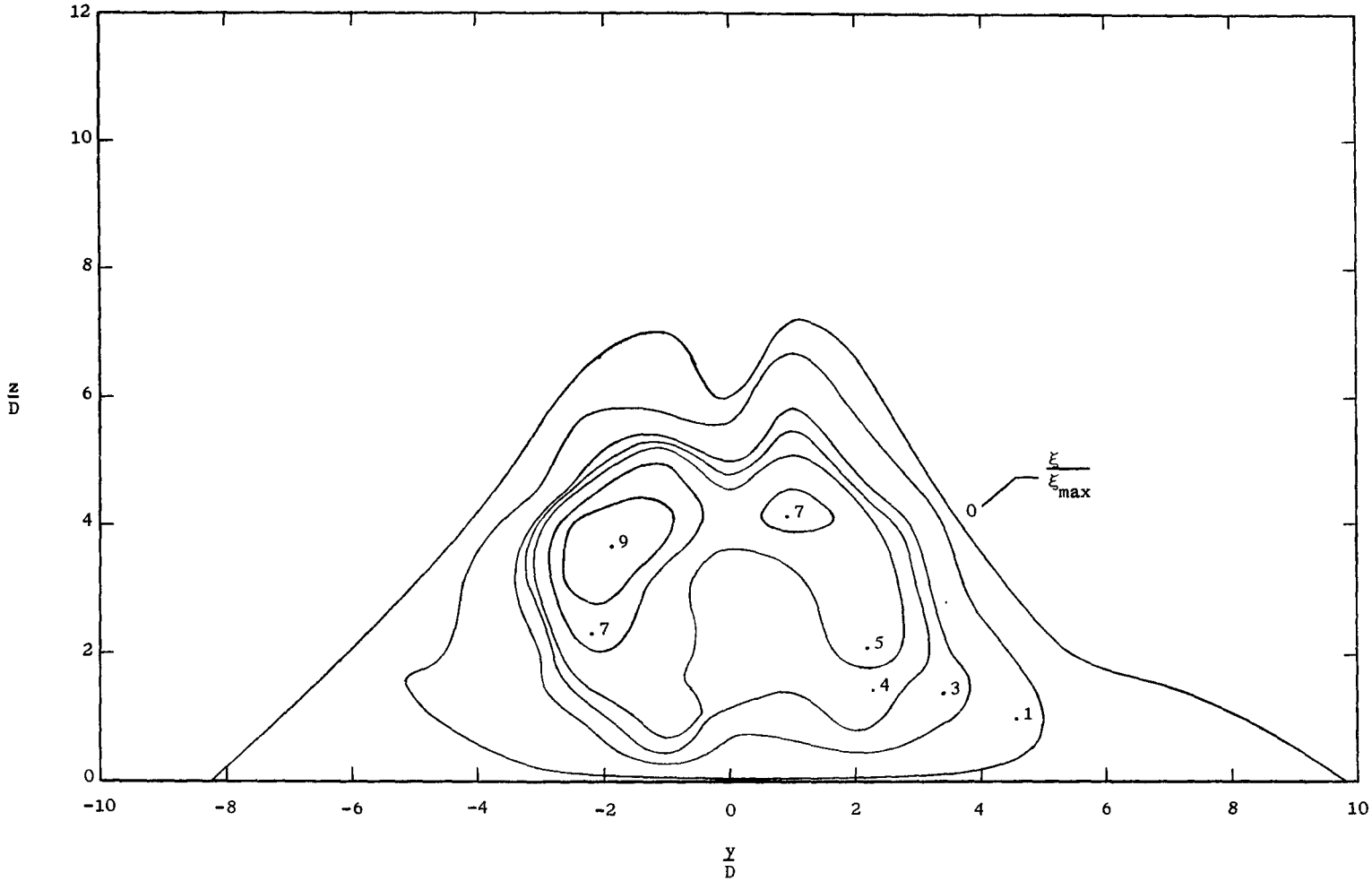

(b) x/D = 15; $p_{t,j}/p_{t,\infty} = 0.34$.

Figure 13.- Continued.

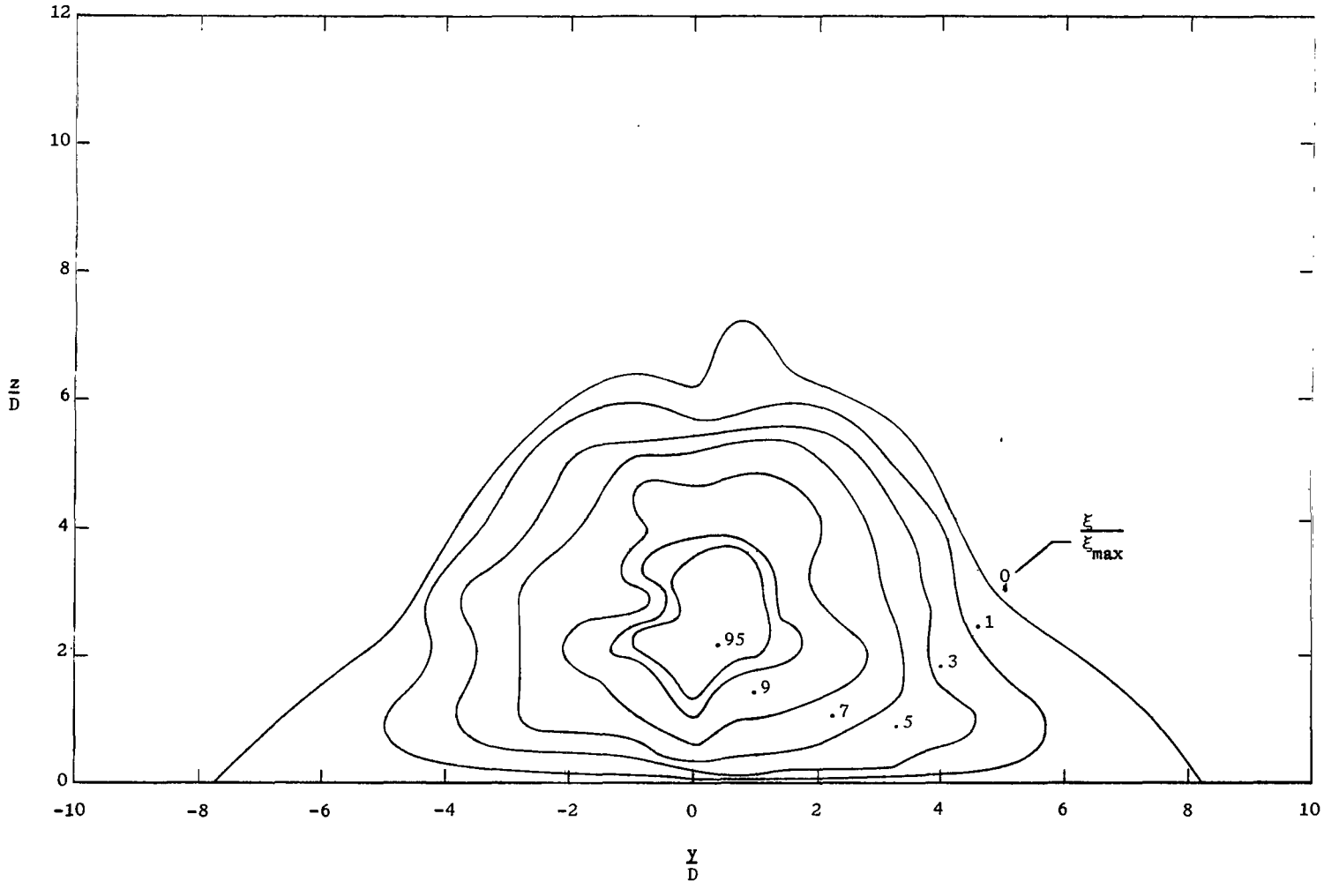

(c) x/D = 30; $p_{t,j}/p_{t,\infty} = 0.34$.

Figure 13.- Continued.

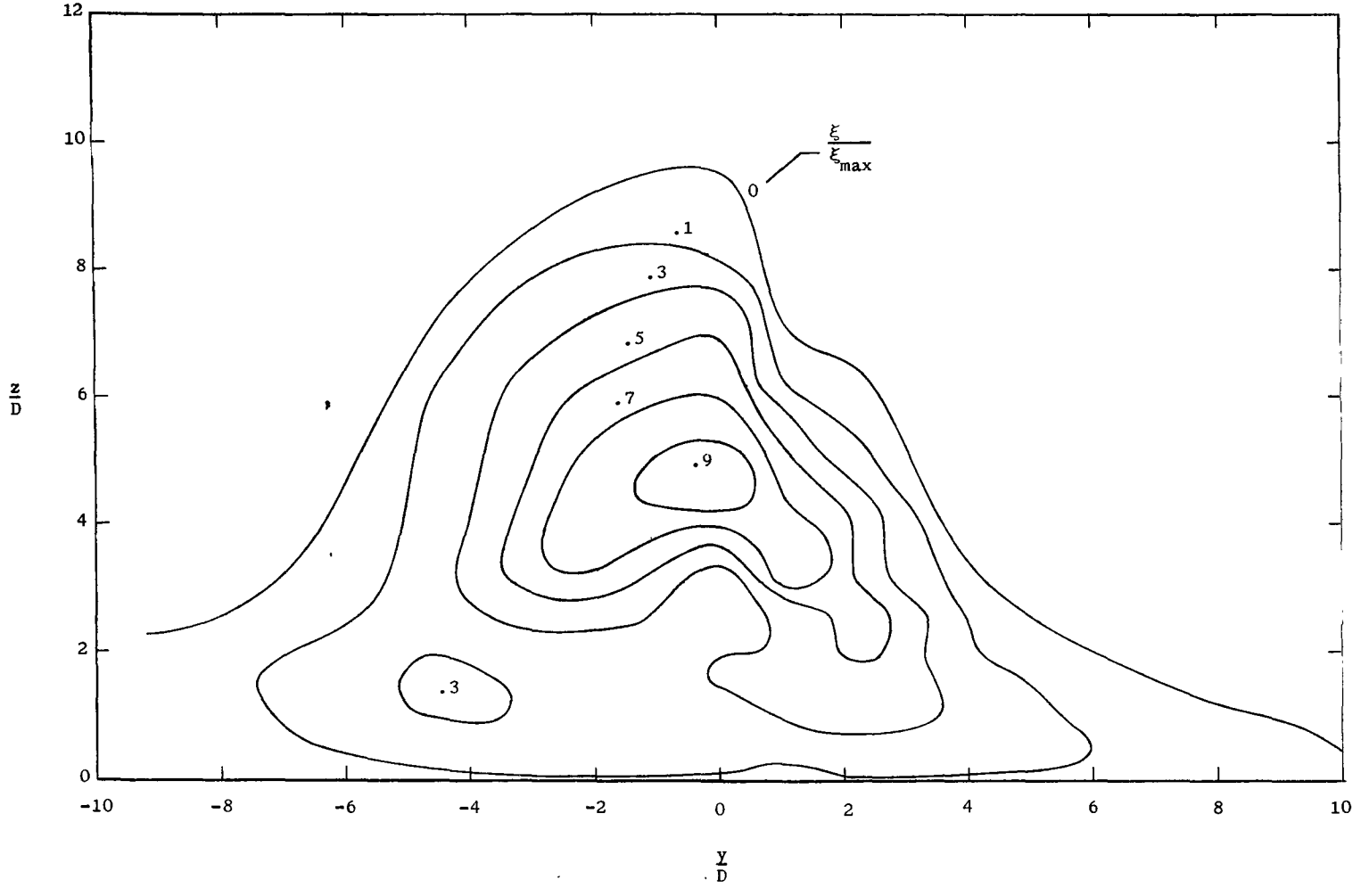

(d) $x/D = 7$; $p_{t,j}/p_{t,\infty} = 0.60$.

Figure 13.- Continued.

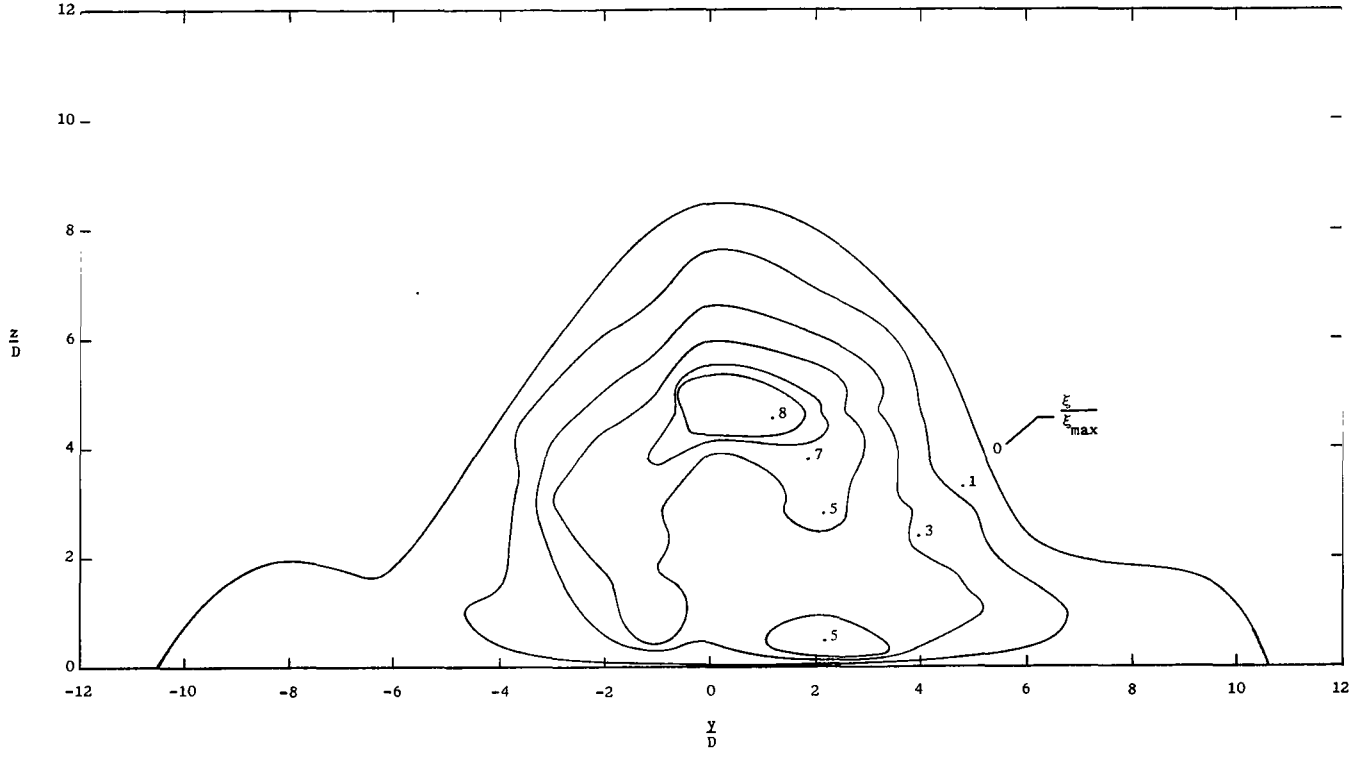

(e) x/D = 15; $p_{t,j}/p_{t,\infty} = 0.60$.

Figure 13.- Continued.

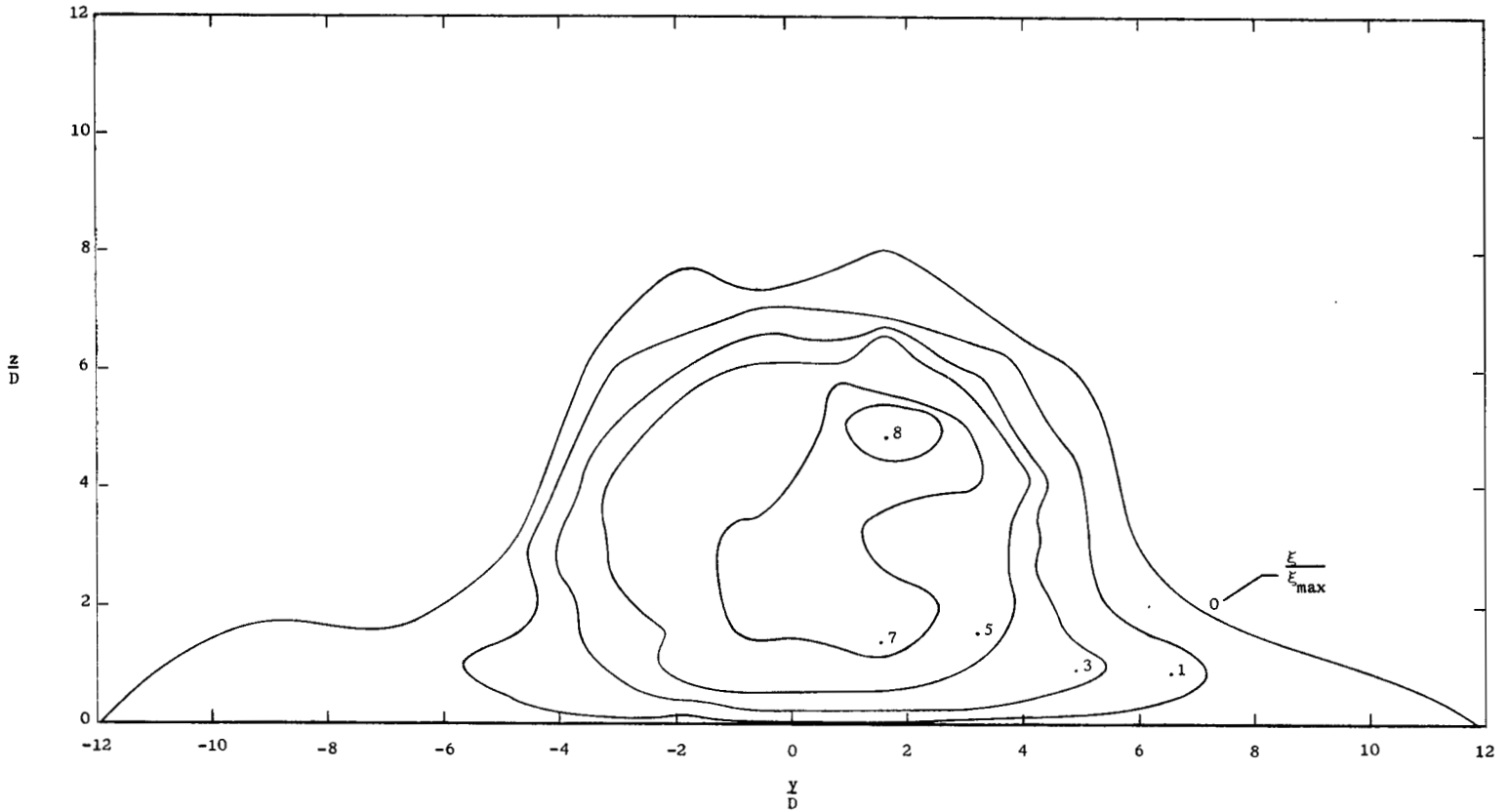

(f) x/D = 30; $p_{t,j}/p_{t,\infty} = 0.60$.

Figure 13.- Concluded.